Mon. Not. R. Astron. Soc. **291,** 162–176 (1997)

# Inverse Compton gamma radiation of faint synchrotron X-ray nebulae around pulsars

F. A. Aharonian,[1★] A. M. Atoyan[1,2★] and T. Kifune[3★]

[1]*Max-Planck-Institut für Kernphysik, Postfach 103980, D-69029 Heidelberg, Germany*
[2]*Yerevan Physics Institute, Alikhanian Brothers 2, 375036 Yerevan, Armenia*
[3]*Institute for Cosmic Ray Research, University of Tokyo, Tanashi, Tokyo 188, Japan*

Accepted 1997 June 6. Received 1997 May 14; in original form 1997 February 15

**ABSTRACT**

The fluxes of the inverse Compton $\gamma$-rays expected from synchrotron X-ray nebulae are calculated and the observability of this radiation is discussed. The main emphasis is given to the pulsar driven nebulae (plerions), although the results and conclusions are equally applicable to the extended non-thermal X-ray sources produced by shock-accelerated electrons in the shell-type supernovae remnants. The existence of the non-thermal (synchrotron) component of X-radiation in these objects implies an effective acceleration of electrons up to energies $E_e \sim 100 B_{-5}^{1/2} \epsilon_{keV}$ TeV ($B_{-5}=B/10^{-5}$ G; $\epsilon_{keV}=\epsilon/1$keV). The inverse Compton scattering of the same electrons on the ambient photon fields may result in observable TeV $\gamma$-radiation as well. The 2.7-K microwave background radiation is, as a rule, the dominant target photon field for production of $\gamma$-rays. This provides a direct relation, for the given magnetic field, between the typical energies of the synchrotron ($\epsilon$) and inverse Compton ($E$) photons produced by the *same* electrons: $\epsilon_{keV} \simeq 0.07 (E/1\ \text{TeV}) B_{-5}$. The ratio of relevant energy fluxes at *these energies* is about $f_\gamma(\geq E)/f_x(\geq\epsilon) \simeq 0.1 B_{-5}^{-2} \xi$, where the $f_x(\geq\epsilon)$ is the energy flux of soft X-rays corrected for absorption, and the factor $\xi \geq 1$ is introduced in order to take into account possible differences in the source sizes responsible for the fluxes observed by X-ray and $\gamma$-ray detectors. Since the fluxes of X-ray nebulae with angular size less than a few arcmin are typically at the level of $f_x \leq 10^{-11}$ erg cm$^{-2}$ s$^{-1}$, then the detectability of these objects in TeV $\gamma$-rays, by current atmospheric Cherenkov telescopes with sensitivities a few times $10^{-12}$ erg cm$^{-2}$ s$^{-1}$, would significantly depend on the ambient magnetic field. In particular, the $\gamma$-ray observability of these X-ray nebulae becomes problematic even for the lowest possible magnetic field, i.e. $B \sim B_{ISM} \simeq 3$–$5$ $\mu$G. Otherwise, the detection of $\gamma$-rays from such sources would require $\xi \gg 1$, which implies that in fact the relativistic electrons occupy a significantly larger region around the accelerator than the $\geq 1$ arcmin X-ray nebulae resolved by the *ROSAT* and *ASCA* satellites. We argue that the invocation of such an hypothesis allows us to explain satisfactorily the flux of TeV $\gamma$-rays detected from the direction of the recently discovered faint X-ray nebula around the pulsar PSR B1706 – 44.

**Key words:** radiation mechanisms: non-thermal – pulsars: individual: PSR B1706 – 44 – gamma-rays: theory – X-rays: stars.

★E-mail: aharon@fel.mpi-hd.mpg.de (FAA); atoyan@fel.mpi-hd.mpg.de (AMA); tkifune@icrr.u-tokyo.ac.jp (TK)

## 1 INTRODUCTION

The search for TeV $\gamma$-rays from pulsars was started some 30 years ago (see, e.g., Weekes 1992). Positive detections of unpulsed radiation at a high confidence level have been reported from the direction of the Crab, PSR B1706 − 44, and possibly the Vela pulsars (for a review, see Kifune 1996a). As for pulsed TeV radiation, despite several claims of possible detections from several objects, in particular, from the Crab pulsar and Geminga (see e.g., Chadwick, McComb & Turver 1990), the results are, as a rule, not straightforward, controversial and biased by the current limitation of detection sensitivity (e.g. Weekes 1992; Kifune 1996a).

At GeV energies, six $\gamma$-ray pulsars have so far been detected by EGRET aboard the *Compton Gamma Ray Observatory*: Crab, Vela, Geminga, PSR B1706 − 44, PSR B1055 − 52 and B1951 + 32 (Nolan et al. 1996), with PSR B0656 + 14 being a possible detection (Ramanamurthy et al. 1996). The modulation of the $\gamma$-ray light curves at the periods known from observations at other wavelengths testifies to the production of $\gamma$-radiation in the pulsar magnetospheres, as the result of non-thermal cascade processes either at the polar cap (e.g. Daugherty & Harding 1982), or in the vacuum gaps at the outer magnetosphere (e.g. Cheng, Ho & Ruderman 1986). Effective $\gamma$-ray production in a pulsar magnetosphere may be extended to the very high energy (VHE) region, $E \geq 100$ GeV, as well, but unfortunately the predictions of fluxes by the current models of $\gamma$-ray pulsars are not sufficiently conclusive (e.g. Cheng 1994). Whether or not the spectra of $\gamma$-ray pulsars continue up to the VHE region is a question which remains one of the interesting issues of high-energy astrophysics.

In addition to the pulsed radiation produced in the magnetosphere, one may expect $\gamma$-rays from extended regions surrounding the pulsars. The pulsars are undisputed sources of relativistic electrons accelerated directly in the magnetosphere and/or by the pulsar wind termination shock (e.g. Arons 1996). The last mechanism seems likely to be responsible for the injection of electrons up to energies $\sim 10^{15}$ eV into the Crab Nebula (Kennel & Coroniti 1984). The synchrotron (S) radiation of these electrons in the nebular magnetic field, calculated in the framework of the MHD model of Kennel & Coroniti (1984), explains the observed non-thermal spectrum over 16 decades of frequency from $10^7$ to $10^{23}$ Hz (Atoyan & Aharonian 1996). The inverse Compton (IC) scattering of the same electrons on the ambient photon fields results in the production of observable VHE $\gamma$-radiation (see, e.g., de Jager & Harding 1992; Atoyan & Aharonian 1996).

This might create, to some extent, an impression that the existence of the bright synchrotron nebula around the Crab pulsar plays a crucial role (as a target photon field) for the production of IC $\gamma$-radiation. In fact, the strong magnetic field in the Crab Nebula ($B > 10^{-4}$ G), which is responsible for intense synchrotron radiation, only reduces the efficiency of $\gamma$-ray production. Indeed, since the energy density of the magnetic field in the Crab Nebula exceeds, by at least two orders of magnitude, the energy density of the photon fields, only $\lesssim 1$ per cent of the energy of accelerated electrons is converted to the IC $\gamma$-rays, the rest being emitted in synchrotron radiation mainly in the form of optical, UV and soft X-ray photons. Thus, the Crab is an effective $\gamma$-ray emitter *not because of the existence of the surrounding nebula*, but as a result of a very high injection rate of relativistic electrons by the pulsar into the nebula, $\dot{L}_e \simeq 5 \times 10^{38}$ erg s$^{-1}$. In fact, the efficiently of IC $\gamma$-ray production could be expected to be significantly higher if the magnetic field were weaker. Remarkably, since the high production rate of TeV IC $\gamma$-rays in the interstellar medium (ISM) can be provided by the 2.7-K microwave background radiation (MBR) alone, a somewhat lower density of optical/infrared photons in the ISM than in the Crab Nebula does not significantly reduce the emissivity of IC $\gamma$-rays. The case of a low ambient magnetic field can be realized, in particular, if the energetic electrons are injected into the ISM by a pulsar which has already left its supernova remnant. Another interesting possibility for a source of the effective formation of intensive IC $\gamma$-ray nebulae around pulsars can be attributed to old pulsars, which would continue to inject relativistic electrons at the late stages, when the remnant has almost disappeared. With reference to this possibility, it is interesting to note the recent paper by Chi, Cheng & Young (1996) who argue about the injection of energetic electrons and positrons into the ISM in time-scales of $\sim 10^5$ yr after the birth of pulsar.

The energy of relativistic electrons, if injected by an isolated pulsar into the conventional regions of the ISM with magnetic field $B_{\rm ISM} \sim 3$–$5$ μG, is released mainly in the form of extended synchrotron (optical to X-ray) and IC ($\gamma$-ray) nebulae (Aharonian 1995; Kifune 1996b). Since the energy densities of the typical interstellar magnetic field and of the 2.7-K background radiation are comparable, the S and IC luminosities are expected to be of the same order of magnitude. The X-ray luminosity of the nebula around an isolated pulsar is expected to be much less than the X-ray luminosity of the Crab Nubula as a result of both lower spin-down luminosities and low ambient magnetic fields in the vicinity of these pulsars. Nevertheless, the modern X-ray detectors like *ROSAT* and *ASCA* have started to allow us to see the faint X-ray nebulae around many pulsars (Kawai & Tamura 1996).

The energy spectrum and the angular distribution of both the X-ray and $\gamma$-ray components depend essentially on the character of propagation of electrons. The parameter $L_0/4\pi d^2$, where $L_0$ is the pulsar spin-down luminosity and $d$ is the distance to the source, might be an indicative of the level of the overall (integrated over the entire extended emission region) X-ray and $\gamma$-ray fluxes, provided that the essential part of the spin-down luminosity of the pulsar (e.g. $\eta \gtrsim 50$ per cent, as in the Crab pulsar) is transferred to relativistic electrons, and the age of the pulsar exceeds the cooling time of $\geq 10$ TeV electrons. As will be shown below, fluxes of TeV $\gamma$-rays at the level of the Crab flux can be predicted from the direction of some isolated pulsars having a parameter $S_0 = L_{37}/d^2_{\rm kpc} \gtrsim 0.1$ (where $L_{37} \equiv L_0/10^{37}$ erg s$^{-1}$ and $d_{\rm kpc} \equiv d/1$ kpc); if they are located in conventional regions of ISM with $B \sim B_{\rm ISM}$.

Note that $S_0$ corresponds to the maximum available radiation flux $f_{\rm max} = L_0/4\pi d^2 \simeq 8.8 \times 10^{-8} S_0$ erg cm$^{-2}$ s$^{-1}$, if all the spin-down luminosity of the pulsar is converted into electromagnetic radiation. The minimum detectable energy fluxes of VHE $\gamma$-rays, by using the current operating or planned imaging atmospheric Cherenkov telescopes, is $\sim 10^{-12}$ erg

cm$^{-2}$ s$^{-1}$. Thus, if we assume that $10^{-2}$–$10^{-3}$ fraction of $L_0$ goes into VHE $\gamma$-rays, we expect a detectable flux of VHE $\gamma$-rays from pulsars with $S_0 = 10^{-3}$–$10^{-2}$. Tens of such pulsars are found in current pulsar catalogues (e.g. Taylor, Manchester & Lyne 1993), and the 30 pulsars with the highest $S_0$ values are listed in Table 1. These pulsars are in order of $S_0$ in the table. As will be discussed later in this paper, the expected luminosity in VHE $\gamma$-rays would not be very far from the X-ray luminosity of the pulsar nebula, which is found to be $10^{-2}$–$10^{-3}$ of $L_0$ for most of the pulsars accompanying nebulae, as shown in Table 1. The pulsar PSR B1055 − 52 is ranked as having the 33rd highest $S_0$ value, but was put into Table 1 rather than two unlisted pulsars with higher $S_0$, because it is a $\gamma$-ray pulsar (Nolan et al. 1996) accompanied by a X-ray nebula (Kawai & Tamura 1996). Table 1 suggests that there are several objects from which VHE $\gamma$-ray fluxes at the level of 0.1 Crab can be expected. However, since this emission is expected to be from relatively extended regions surrounding the pulsar, the source detectability depends essentially on the angular size of the emission region and the character of propagation of relativistic electrons. In principle, the propagation and confinement of energetic electrons in the nebula is defined by several parameters such as the strength and structure of the magnetic field, the level of turbulence, etc. All those parameters not only depend on pre-supernova (generally unknown) conditions, but also are strongly affected by the pulsar itself. In the case of strong sources such as the Crab pulsar ($L_0 \simeq 5 \times 10^{38}$ erg s$^{-1}$), the nebular magnetic field can exceed, by a factor of 100, the interstellar magnetic field. However, for most pulsars $L_0 \leq 10^{37}$ erg s$^{-1}$, thus the amplifications of the ambient magnetic field could take place in much smaller scales. Apparently, the ratio of IC $\gamma$-ray to synchrotron X-ray luminosities $L_\gamma/L_x$ at different angular distances from the pulsar carries almost model-independent information on the strength and spatial distribution of the magnetic field within 1 to 10 pc.

**Table 1.** Pulsars with highest $S_0$ values.

| (1) name | (2) p | (3) log $L_0$ | (4) log $\tau$ | (5) d | (6) log $S_0$ | (7) log $L_X$ | (8) size | (9) | (10) |
|---|---|---|---|---|---|---|---|---|---|
| B0531+21 | 33.4 | 38.65 | 3.10 | 2.0 | 1.05 | 37.18 | 0.6 | a | Crab |
| B0833−45 | 89.3 | 36.84 | 4.05 | .5 | 0.44 | 34.08 | >3 | a | Vela |
| J0633+1746 | 237.1 | 34.51 | 5.53 | .15 | -0.84 | 30.43 | >0.9 | a | Geminga |
| B1706−44 | 102.4 | 36.53 | 4.24 | 1.8 | -0.98 | 33.1 | <1 | b | |
| B1509−58 | 150.7 | 37.25 | 3.19 | 4.4 | -1.04 | 34.8 | ~6 | c | MSH15-52 |
| J0437−4715 | 5.8 | 34.07 | 9.20 | .14 | -1.22 | | | | binary pulsar |
| B1951+32 | 39.5 | 36.57 | 5.03 | 2.5 | -1.23 | 33.82 | >10 | a, d | CTB80 |
| B1046−58 | 123.7 | 36.30 | 4.31 | 3.0 | -1.65 | 32.93 | 9 | a | 2EGJ1049-5847? |
| B1823−13 | 101.5 | 36.45 | 4.33 | 4.1 | -1.78 | <33.9 | <5 | e | 2EGJ1825-1307? |
| B1800−21 | 133.6 | 36.35 | 4.20 | 3.9 | -1.83 | | | | W30 |
| B1929+10 | 226.5 | 33.59 | 6.49 | .17 | -1.87 | 30.58 | 0.8 | a | |
| B1757−24 | 124.9 | 36.41 | 4.19 | 4.6 | -1.92 | | | | G5.4-1.2 W28 |
| B1937+21 | 1.6 | 36.04 | 8.37 | 3.6 | -2.07 | | | | |
| B1821−24 | 3.1 | 36.35 | 7.48 | 5.5 | -2.13 | | | | |
| B1727−33 | 139.4 | 36.09 | 4.42 | 4.2 | -2.16 | | | | |
| B1957+20 | 1.6 | 35.21 | 9.18 | 1.5 | -2.16 | | | | eclipsing binary |
| B0656+14 | 384.9 | 34.58 | 5.04 | .76 | -2.18 | 31.62 | 2.7 | a | Monogem |
| B0540−69 | 50.4 | 38.17 | 3.22 | 49.4 | -2.22 | | | | |
| B1257+12 | 6.2 | 34.27 | 8.94 | .62 | -2.30 | | | | |
| B0114+58 | 101.4 | 35.35 | 5.44 | 2.1 | -2.30 | | | | |
| J2043+2740 | 96.1 | 34.75 | 6.08 | 1.1 | -2.33 | | | | |
| J0034−0534 | 1.9 | 34.60 | 9.65 | .98 | -2.38 | | | | |
| B0740−28 | 166.8 | 35.16 | 5.20 | 1.9 | -2.40 | | | | |
| B1853+01 | 267.4 | 35.63 | 4.31 | 3.3 | -2.41 | ~33.6 | <5 | f | W44, 2EJ2857+011 |
| B1259−63 | 47.8 | 35.92 | 5.52 | 4.6 | -2.41 | | | | binary pulsar |
| B0950+08 | 253.1 | 32.75 | 7.24 | .12 | -2.41 | | | | |
| B1610−50 | 231.6 | 36.20 | 3.87 | 7.3 | -2.53 | 34.65 | 25 | a | Kes 32 |
| B1338−62 | 193.3 | 36.14 | 4.08 | 8.7 | -2.74 | | | | G308.8-01 |
| B1830−08 | 85.3 | 35.77 | 5.17 | 5.7 | -2.74 | | | | |
| B1055−52 | 197.1 | 34.48 | 5.73 | 1.5 | -2.87 | 32.30 | 3 | a | |

(1) Pulsar name (we put known pulsars in the order of $S_0$, spin-down luminosity $L_0$ divided by the square of distance $d$, in units of $10^{37}$ erg s$^{-1}$ kpc$^{-2}$), (2) period in ms, (3) spin-down luminosity $L_0$ in erg s$^{-1}$, (4) age $\tau$ in year, and (5) distance in kpc. Values for (3), (4) and (5) are from Taylor, Manchester & Lyne (1993). (b) $S_0 = L_{37}/d^2_{kpc}$ (kpc) defined in the text. (7) X-ray luminosity of accompanied nebula $L_X$ in erg s$^{-1}$. (8) Size of X-ray nebula in pc. (7) and (8) are given in or estimated from the references in the column (9). (10) Other names, or accompanying feature. The references in column (9) are: (a) Shibata, Kawai & Tamura (1997); (b) Becker, Brazier & Trümper (1995); (c) Tamura et al. (1996); (d) Safi-Harb, Ögelman & Finley (1995); (e) Finley, Srinivasan & Park (1996); (f) Harrus, Hughes & Helfand (1996).

## 2 SYNCHROTRON VERSUS INVERSE COMPTON: QUALITATIVE ANALYSIS

Suppose that relativistic electrons are captured in a region characterized by a magnetic field $B$ and a photon field of energy density $w_{\rm ph}$, and assume that the radiative energy losses of electrons due to synchrotron and inverse Compton processes dominate over other possible losses like bremsstrahlung, adiabatic, etc. Thus the lifetime of electrons is determined as

$$t_{\rm r}(E_{\rm e})=\left(\frac{4}{3}\,\sigma_{\rm T}cw_0E_{\rm e}/m_{\rm e}^2c^4\right)^{-1}=3.1\times10^5$$
$$\times\,(E_{\rm e}/1\ {\rm TeV})^{-1}(w_0/1\ {\rm eV\ cm^{-3}})^{-1}\ {\rm yr}, \qquad (1)$$

where $w_0=w_B+w_{\rm ph}$, and $w_B=B^2/8\pi$. Here we discuss the magnetic fields in the range from $B\sim3\times10^{-4}$ G (the average magnetic field in the Crab Nubula) down to $B\sim3\times10^{-6}$ G typical for ISM. The photon energy density in the regions surrounding the pulsars is contributed by several radiation fields including (1) 2.7-K MBR, (2) diffuse galactic dust far-infrared (FIR) and starlight near-infrared/optical backgrounds, and (3) possible intensive radiation fields of local origin.

Although the energy density of the diffuse galactic radiation exceeds by a factor of a few the energy density of the 2.7-K MBR, its importance is strongly reduced in the energy region above 100 GeV due to the Klein–Nishina effect. Therefore the only photon field which remains an important target for production of the VHE $\gamma$-rays is 2.7-K radiation (see Section 3). This circumstance allows us to derive rather simple and useful relations between the frequencies and fluxes of the synchrotron X-rays and IC $\gamma$-rays. In this section we present these relations, which may be helpful for a better understanding of the results of numerical calculations carried out for different source scenarios discussed in the following sections.

For the total energy $W_{\rm e}(E_{\rm e})\,{\rm d}E_{\rm e}$ contained in electrons within the region $(E_{\rm e}, E_{\rm e}+{\rm d}E_{\rm e})$, the S and IC luminosities can be expressed as

$$L_{\rm i}(E_{\rm i})\,{\rm d}E_{\rm i}\sim\frac{W_{\rm e}(E_{\rm e})\,{\rm d}E_{\rm e}}{t_{\rm i}(E_{\rm e})}, \qquad (2)$$

where $t_{\rm i}$ is the radiative cooling time of electrons due to the synchrotron (i=S) or inverse Compton (i=IC) processes, and $E_{\rm i}$ is the characteristic energy of the photons produced by the electrons with energy $E_{\rm e}$.

The $\delta$-functional approximation for the S and IC cross-sections (e.g. Ginzburg 1979) allows us to connect the energy $E_{\rm e}$ of the parent electron with the characteristic energy of the synchrotron ($\epsilon$) and IC ($E$) photons: $\epsilon\simeq h\nu_{\rm c}/3$, where $\nu_{\rm c}=1.5(eB\sin\psi/2\pi m_{\rm e}c)(E_{\rm e}/m_{\rm e}c^2)^2$, and (for IC scattering in the Thomson limit) $E\simeq(4/3)h\nu_0(E_{\rm e}/m_{\rm e}c^2)^2$, where $h\nu_0$ is the energy of the target photons. Then, substituting $\sin\psi\rightarrow\sqrt{2/3}$ (the case of isotropical pitch angles $\psi$), we obtain

$$\epsilon\simeq0.2B_{-5}(E_{\rm e}/1\ {\rm TeV})^2\ {\rm eV}, \qquad (3)$$

where $B_{-5}\equiv B/10^{-5}$ G, and

$$E\simeq5(h\nu_0/10^{-3}\ {\rm eV})(E_{\rm e}/1\ {\rm TeV})^2\ {\rm GeV}. \qquad (4)$$

For the MBR having narrow Planckian distribution, $h\nu_0$ can be taken, with good accuracy, to be equal to the mean energy of the target photons $h\bar{\nu}_0=2.7kT\simeq6\times10^{-4}$ eV. Thus, for effective production of the IC $\gamma$-rays with $E\sim1$ TeV on MBR, one needs electrons with $E_{\rm e}\simeq20$ TeV.

Equations (3) and (4) allow us to connect the characteristic energies of S and IC photons produced by the same electrons,

$$\epsilon\simeq0.07(E/1\ {\rm TeV})B_{-5}\ {\rm keV}. \qquad (5)$$

Therefore, for the characteristic magnetic fields of the plerions $B$ around $10^{-5}$–$10^{-4}$ G there should be direct correlation between the soft X-ray ($\leq1$ keV) and TeV $\gamma$-ray fluxes.[1]

From equations (1) and (2), it follows that the ratio of the energy fluxes $f_{\rm i}(E_{\rm i})=I_{\rm i}(E_{\rm i})\times E_{\rm i}^2$ [where $I(E)$ is for the differential photon fluxes] of the S and IC photons in the energy ranges coupled by equation (5), is

$$\frac{f_{\rm IC}(E)}{f_{\rm S}(\epsilon)}=\frac{L(E)\,{\rm d}E}{L(\epsilon)\,{\rm d}\epsilon}=\frac{w_{\rm ph}}{w_{\rm B}} \qquad (6)$$

(here we take into account that, according to equation 5, ${\rm d}E/{\rm d}\epsilon=E/\epsilon$).

Note that equation (6) is obtained (1) in the $\delta$-functional approximation of the synchrotron and IC cross-sections, and (2) assuming that the IC scattering takes place in the Thomson regime. In order to estimate the accuracy of this approach, in Fig. 1 we show the ratio $R_\delta(E)=[w_{\rm B}f_{\rm IC}(E)]/[w_{\rm ph}f_{\rm S}(\epsilon)]$ calculated numerically using exact S and IC cross-sections for different spectra of the relativistic electrons. The curves plotted in the solid, dashed and dot–dashed lines are for the pure power-law spectra of electrons $N(E_{\rm e})\propto E_{\rm e}^{-\alpha_{\rm e}}$ with $\alpha_{\rm e}=2$, 3 and 4, respectively. It is seen that, while for $\alpha_{\rm e}=3$ the results obtained in the $\delta$-functional approximation coincide with the results of numerical calculations (i.e. $R_\delta=1$), for other values of $\alpha_{\rm e}$ there is some deviation from the exact calculations, although this does not exceed $\pm20$ per cent. Moreover, even for irregular (such as broken-power law) electron spectra, the $\delta$-functional approximation provides a reasonable accuracy (see dotted curve in Fig. 1), quite sufficient for qualitative estimates up to energies $E\sim1$ TeV. At higher energies the impact of the Klein–Nishina effect becomes noticeable, though even at $E\simeq10$ TeV the Thomson cross-section still provides an accuracy $\sim50$ per cent. Thus equations (5) and (6) can be recommended for qualitative predictions of the IC $\gamma$-ray fluxes based on the observed synchrotron fluxes from the non-thermal X-ray nebulae.

Note, however, that predictions of this kind should in general be treated rather cautiously, since for the given ambient magnetic field $B$ a model-independent estimate of the TeV $\gamma$-ray fluxes is possible only if the fluxes of the synchrotron radiation at certain energies $\epsilon$ given by equation (5) are known. Indeed, as it follows from equation (5),

[1] A relation analogous to equation (5) was given in de Jager (1996). Note, however, that there is an essential discrepancy, by a factor of $\sim3$, in the coefficients relating $E$ and $\epsilon$, which perhaps results from using the value $\epsilon=h\nu_{\rm c}$ for the characteristic synchrotron photon energy of de Jager (1996), instead of for the mean photon energy $\epsilon=0.3h\nu_{\rm c}$ (see e.g. Ginzburg 1979).

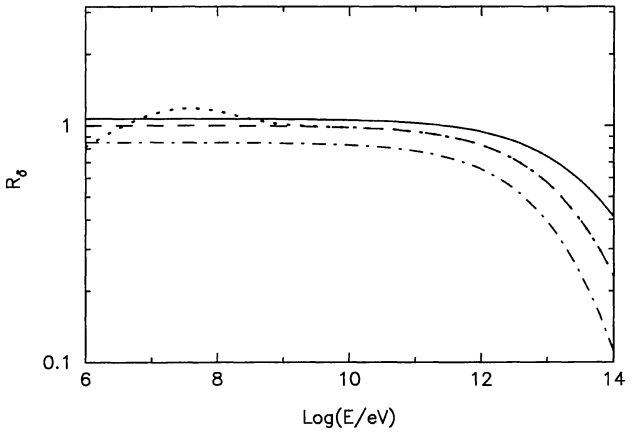


**Figure 1.** The accurate numerical calculations of the ratio $R_\delta(E)=[w_B f_{IC}(E)]/[w_{MBR} f_S(\epsilon)]$ for the energy fluxes of the IC and S photons $[f_i(E_i)=I(E_i)\times E_i]$ normalized to the energy densities of the magnetic and MBR fields, taken at energies $E$ and $\epsilon$ related by equation (5). The solid, dashed, and dot–dashed curves are calculated for the pure power-law prompt spectrum of relativistic electrons $N(E_e)\propto E^{-\alpha_e}$ with the index $\alpha_e=2$, 3 and 4, respectively. The dotted curve is calculated for the broken power-law spectrum with $\alpha_e=0$ at $E_e\le E_c=100$ GeV and $\alpha_e=3$ at $E_e\ge E_c$.

only for magnetic field $B\ge 5\times 10^{-4}$ G does the energy of the synchrotron photons, $\epsilon$, become larger than 1 keV. Meanwhile, for more probable nebular fields $B\sim 10^{-5}$ G, the energy of the synchrotron photons corresponding to 1 TeV IC $\gamma$-rays is in the UV range, which as a rule is not available. In this case the correspondence between keV X-ray and TeV $\gamma$-ray fluxes becomes strongly model-dependent, and thus requires detailed numerical calculations which should take into account the injection spectrum, energy losses, and propagation of electrons.

## 3 BROAD-BAND SPECTRAL FEATURES OF THE NON-THERMAL X-RAY NEBULAE

### 3.1 The spectrum of electrons: general formalism

There are only a few parameters which define the fluxes of the synchrotron and IC radiation observable over more than 20 decades of frequencies from $10^7$ Hz to $\nu\ge 10^{27}$ Hz, the principal ones being the magnetic and photon fields, as well as the 'prompt' spectrum of relativistic electrons. The latter in its turn depends on the electron injection spectrum and character of evolution of the source.

The spectrum $N\equiv N(E_e, t)$ of relativistic electrons at instant $t$ is defined by the equation (e.g. see Ginzburg & Syrovatskii 1964)

$$\frac{\partial N}{\partial t}=\frac{\partial}{\partial E_e}[PN]-\frac{N}{\tau}+Q, \tag{7}$$

where $Q\equiv Q(E_e, t)$ is the electron injection rate, $P\equiv P(E_e)$ is the energy-loss rate, and $\tau\equiv\tau(E_e)$ is the escape time of the electrons from the nebula. Assuming $\delta$-functional injection at an instant $t_1$, i.e. $Q(E_e, t)=Q_1(E_e)\,\delta(t-t_1)$, one finds the Green-function solution $G(E_e, t, t_1)$ for arbitrary injection spectrum $Q_1(E_e)\equiv Q(E_e, t_1)$, if considering equation (7) at $t>t_1$ (i.e. a uniform linear equation) with initial condition $G(E_e, t=t_1, t_1)=Q_1(E_e)$. The complete Green-function solution [i.e. for $Q_1(E_e)=\delta(E_e-E_1)$] in the case of energy-independent escape, $\tau(E_e)=$constant, is given in Ginzburg & Syrovatskii (1964). For an arbitrary $\tau(E_e)$ and arbitrary $Q_1(E_e)$ the Green-function solution to equation (7) at $t\ge t_1$ is

$$G(E_e, t, t_1)=\frac{P(\zeta_t)Q_1(\zeta_t)}{P(E_e)}\exp\left[-\int_{t_1}^{t}\frac{dx}{\tau(\zeta_x)}\right], \tag{8}$$

where $\zeta_t$ depends on $t-t_1$ and $E_e$, and is found from the equation

$$t-t_1=\int_{E_e}^{\zeta_t}\frac{dE}{P(E)}. \tag{9}$$

The variable $\zeta_t$ corresponds to the initial energy of an electron at instant $t_1$ which is cooled down to given energy $E_e$ by the instant $t$. Note that $\zeta_{t_1}=E_e$, and $d\zeta_t/dt=P(\zeta_t)$. Integration of $G(E_e, t, t_1)$ over $dt_1$ gives the general solution to equation (7)

$$N(E_e, t)=\frac{1}{P(E_e)}\int_{-\infty}^{t}P(\zeta_t)Q(\zeta_t, t_1)\exp\left(-\int_{t_1}^{t}\frac{dx}{\tau(\zeta_x)}\right)dt_1. \tag{10}$$

In the numerical calculations below we suppose a stationary (at $t\ge 0$) injection spectrum of electrons in the form of a broken power-law function, and an exponential cut-off in the region of maximum acceleration energies $E\sim E_0$,

$$Q(E_e)=A\exp\left(-\frac{E_e}{E_0}\right)\begin{cases}(E_e/E_c)^{-\alpha_0}, & \text{if } E_e\le E_c\\ (E_e/E_c)^{-\alpha_e}, & \text{if } E_e\ge E_c\end{cases}. \tag{11}$$

The particular case of $E_c\sim m_e c^2$ (or $\alpha_0=\alpha_e$) corresponds to the case of a single power-law injection spectrum which can be provided e.g. by the conventional shock acceleration in the shell-type supernova remnants. Assumption of $\alpha_0\le 0$ and high values of $E_c$ up to $\le 1$ TeV allows us to reduce, if necessary, the energy requirements of the injection rate of relativistic electrons without any impact on the X-ray and TeV $\gamma$-ray fluxes. Moreover, this kind of electron spectrum injected in the post-shock regions in the pulsar wind termination shocks seems to be more appropriate for the pulsar-driven nebulae (Arons 1996). Besides, the injection spectrum in the form of equation (11) with $E_c\to E_0$ allows us to analyse also the case of rather narrow ($\Delta E_e\sim\bar{E}_e$) injection spectra, which presumably can be realized in the case of weak nebular shocks which would not be able to significantly redistribute the monoenergetic spectrum of electrons in the relativistic wind in the upstream region of the shock.

### 3.2 Target photon fields

In order to demonstrate the impact of uncertainties in the background photon fields on the IC $\gamma$-ray fluxes, in Fig. 2(a) we show the contributions of four different target photon fields into the total IC flux, assuming that a pulsar somehow accelerates and injects electrons (e.g. through the relativistic wind) with a constant power $L_e=10^{37}$ erg s$^{-1}$ during the

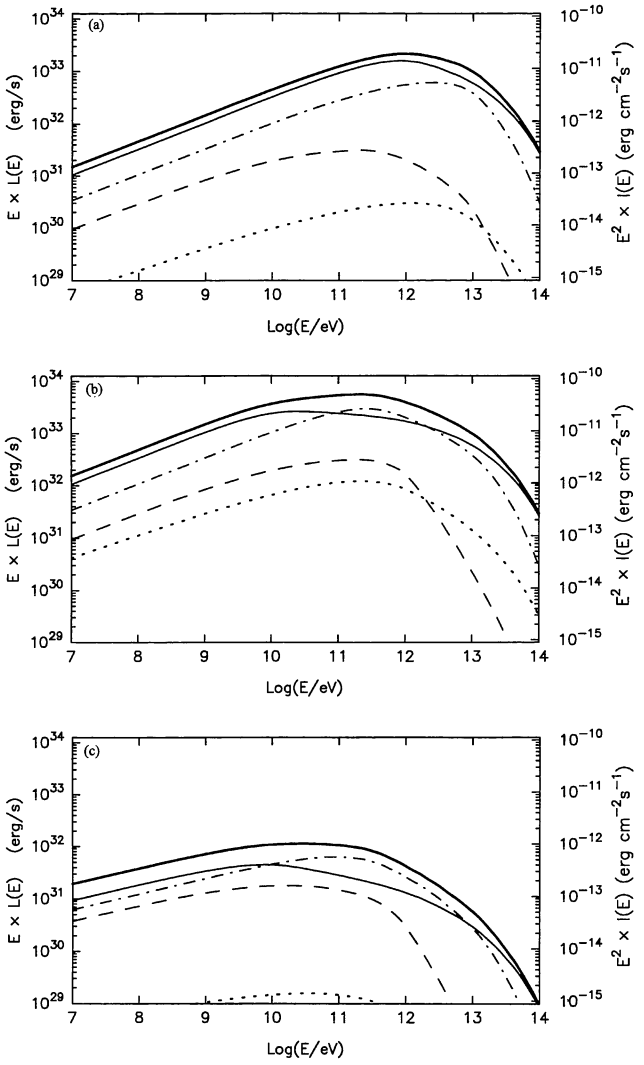


**Figure 2.** (a) The contributions of different target photon fields to the production of IC $\gamma$-rays: 2.7-K MBR (solid line); FIR with $w_{\rm FIR}=0.5$ eV cm$^{-3}$ and $T=100$ K (dot–dashed line); NIR/optical with $w_{\rm sl}=1$ eV cm$^{-3}$ and $T=5000$ K (dashed line); synchrotron-self-Compton radiation produced by relativistic electrons for the source size $r_0=2$ pc and magnetic field $B=3\times10^{-5}$ G (dotted line). The heavy solid line corresponds to the overall spectrum of IC $\gamma$-rays. The injection spectrum of relativistic electrons in the form of equation (11), with $E_{\rm c}=m_{\rm e}c^2$, $E_0=100$ TeV, $\alpha_{\rm e}=2$, and total injection rate $L_{\rm e}=10^{37}$ erg s$^{-1}$ are supposed. The age of the pulsar $t_0=10^3$ yr. The right-hand-side axis is scaled to the energy fluxes expected for the distance to the pulsar $d=1$ kpc. (b) Same as (a) except for the age of the pulsar, $t_0=10^4$ yr. (c) Same as (a) except for the age of the pulsar, $t_0=10^4$ yr, and the power-law index of electrons $\alpha_{\rm e}=2.4$.

age of the pulsar of $t_0=10^3$ yr into the surrounding medium with $B=3\times10^{-5}$ G.

Formally, the target photon fields can be subdivided into two groups, namely, (1) the *external* galactic and extragalactic photon fields, and (2) the *internal* radiation produced by the source itself. The most important extragalactic field for production of IC $\gamma$-rays is the 2.7-K MBR. The contribution of the galactic background radiation is essentially the result of the dust and starlight photons with peak intensity at wavelengths $\lambda\sim100$ and $\sim1$ μm, respectively. While the density of the MBR is universal, with $w_{\rm MBR}=0.25$ eV cm$^{-3}$, the density of both of the galactic background fields varies from site to site, with average values being $w_{\rm FIR}\sim0.05$ eV cm$^{-3}$ and $w_{\rm sl}\sim0.5$ eV cm$^{-3}$ (see e.g. Mathis, Metzger & Panagia 1983). Since plerions are located near the galactic plane, this may lead, in principle, to uncertainties in the calculated IC $\gamma$-ray fluxes. However, fortunately these uncertainties turn out not to be crucial. Indeed, as it follows from Fig. 2(a), even for densities of the dust FIR and starlight radiations $w_{\rm FIR}=0.5$ eV cm$^{-3}$ and $w_{\rm sl}=1$ eV cm$^{-3}$, which are respectively 10 and two times higher than the averaged galactic disc values, the IC scattering of electrons on the 2.7-K MBR dominates at all energies of $\gamma$-rays. Since it is rather difficult to speculate with such dramatic gradients of the diffuse galactic background even in very bright regions of the galactic disc, one may neglect with rather high confidence the contribution of these two target photon fields.

Meanwhile, FIR emission significantly exceeding the diffuse galactic level can be attributed to the internal radiation of the source itself. The level of $w_{\rm FIR}=0.5$ eV cm$^{-3}$ used in Fig. 2(a) corresponds to the FIR density in the Crab Nebula with characteristic dust temperature $\simeq100$ K (Marsden et al. 1984). Note, however, that the Crab is a unique source, and there are no reasons to assume that other nebulae possess such a high intrinsic FIR density, which implies very high source luminosity $L_{\rm FIR}\simeq3\times10^{36}(r/1\ {\rm pc})^2$ erg s$^{-1}$, where $r$ is the radius of the FIR production region.

Another peculiarity of the Crab Nebula which distinguishes this source from other plerions is the very high density of the synchrotron radiation field. In particular, the photons of this origin at the wavelengths from radio to FIR provide a contribution to the IC $\gamma$-ray flux of the Crab which is comparable with the contributions from both dust FIR and 2.7-K MBR target photon fields (Aharonian & Atoyan 1995). However, the high density of synchrotron radiation in the Crab Nebula is due both to the exceptionally high spin-down luminosity of the Crab pulsar (see Table 1) which with almost 100 per cent efficiency is converted to relativistic electrons, and to the high nebular magnetic field, $B>10^{-4}$ G (e.g. Kennel & Coroniti 1984). As is seen in Fig. 2(a), in the case of the modest injection rate of relativistic electrons by most pulsars and/or weaker B-field, the contribution of the synchrotron photons to the production of IC $\gamma$-rays is negligible by many orders of magnitude.

Concerning the contribution of the FIR to the production of IC $\gamma$-rays (compared with that of the 2.7-K field), we should note that this contribution increases for a steeper spectrum of electrons. This is connected with the enhancement of the lower (few TeV) energy in a steep electron spectrum which are not able to produce TeV $\gamma$-rays on 2.7-K MBR, but still are able to produce TeV $\gamma$-rays on FIR. For a blackbody (Planckian) distribution of the target photons the emissivity of the IC $\gamma$-rays in the Thomson limit is $q(E)\propto\zeta T_{\rm r}^{(\alpha_{\rm e}+5)/2}E^{-(\alpha_{\rm e}+1)/2}$ (Blumenthal & Gould 1970), where $T_{\rm r}$ and $\zeta$ are the temperature and the dilution factor of the thermal radiation, and $\alpha_{\rm e}$ is the power-law index of the prompt electron spectrum. Since the background radiations are usually given in terms of the temperature $T_{\rm r}$ and radiation energy density $w_{\rm r}=A\zeta\sigma_{\rm S-B}T_{\rm r}^4$, it is convenient to present the $\gamma$-ray emissivity in the following form:

$$q(E) \propto w_r T_r^{(\alpha_e-3)/2} E^{-(\alpha_e+1)/2}. \quad (12)$$

This expression allows us to easily compare the relative contributions of different thermal photon fields as $q_1(E)/q_2(E) = (w_1/w_2)(T_1/T_2)^{(\alpha_e-3)/2}$ as long as the production of IC $\gamma$-rays remains in the Thomson regime. It is interesting to note that for the prompt electron spectrum with $\alpha_e = 3$, the ratio of IC emissivities in two different background photon fields is determined simpy by the ratio of energy densities. For other values of $\alpha_e$ the relative contributions of different target photon fields essentially depend on the radiation temperatures as well. In particular, for the electron spectra with $\alpha_e = 2$ the contribution of the dust FIR with $T_{FIR} \simeq 100$ K may be comparable with the one of the 2.7-K photons if $w_{FIR} \geq 1.5$ eV cm$^{-3}$.

The contribution of the high-temperature thermal radiations to the IC $\gamma$-ray production may become non-negligible for steep electron spectra with $\alpha_e \geq 3$. (Note, however, that for VHE $\gamma$-ray production on near-infrared/optical photons even very steep electron spectra cannot compensate for the strong suppression due to the Klein–Nishina cross-section.) Steep prompt spectra of relativistic electrons can be attributed to a steep injection spectrum and/or to significant energy losses of VHE electrons during the lifetime of the source (i.e. when $t_r \leq t_0$). The results of calculations for both these cases are shown in Figs 2(b) and (c). As follows from these figures, in the VHE $\gamma$-ray domain the contribution of the FIR may dominate over the contribution from the MBR. Thus, in the case of IC scattering of relativistic electrons with very steep spectra in a nebulae with a level of FIR not much less than that in the Crab Nebula, the IC upscattering of the FIR photons should be taken into account, along with the contribution from the MBR photons. However, in most cases the contribution from all target photon fields discussed above, except for the MBR, can be neglected without significant impact on the accuracy of calculations.

### 3.3 The effect of the magnetic field

The fluxes and the spectral shape of both synchrotron and IC radiation depend on the prompt spectrum of electrons $N(E_e)$, which in its turn is defined by the injection spectrum $Q(E)$ and the energy-loss rate of the electrons. In the case of low magnetic fields comparable with the ISM magnetic field, $B_{ISM} \sim (3\text{–}5) \times 10^{-6}$ G, both synchrotron and IC (on the MBR and diffuse galactic radiation) processes, with $w_0 = B^2/8\pi + w_{ph} \sim 1$ eV cm$^{-3}$ equally contribute to the total energy losses. Correspondingly, in this regime the energy released in the synchrotron and IC radiation are comparable. However, when the magnetic field in the source noticeably exceeds $B_{ISM}$, then the total energy loss is determined by the synchrotron process, which leads to a strong imbalance between the energies released in synchrotron and IC channels. This is seen in Fig. 3(a), where the calculated luminosities of a nebula with different B-fields are shown. We assume that a $10^4$-yr-old pulsar continuously injects into the nebula relativistic electrons with luminosity $L_e = 10^{37}$ erg s$^{-1}$. In order to show clearly the effect of the steepening of the electron spectrum due to the radiative energy losses, in this figure we suppose a very high value of $E_0 = 10^3$ TeV. In Fig. 4 we present the relevant electron spectra $N(E_e, t = 10^4$ yr) for the magnetic fields and other parameters corresponding to the ones in Fig. 3(a). Note that for $B = 3 \times 10^{-6}$ G, when the energy densities of the magnetic and photon fields are almost equal, the energies

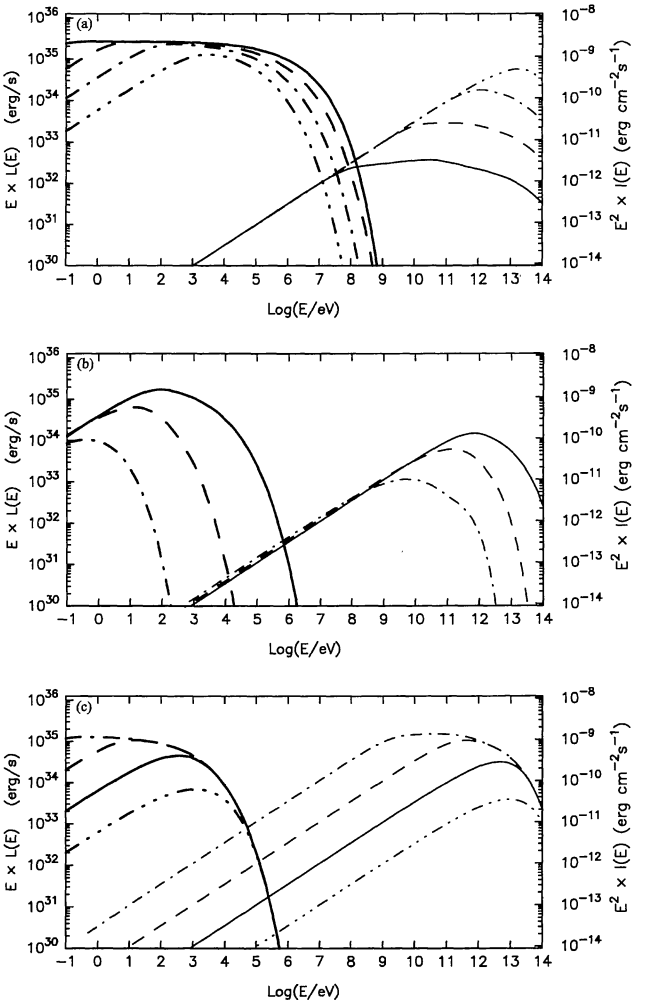


**Figure 3.** (a) The spectra of the S and IC radiations of the nebula for different ambient magnetic fields: $B = 10^{-4}$ G (solid lines), $B = 3 \times 10^{-5}$ G (dashed lines), $B = 10^{-5}$ G (dot–dashed lines), and $B = 3 \times 10^{-6}$ G (three-dot–dashed lines). It is assumed that the $10^4$-yr-old pulsar stationarily injects relativistic electrons into the nebula with $L_e = 10^{37}$ erg s$^{-1}$. The parameters of the injection spectrum in equation (11) are $E_c = m_e c^2$, $E_0 = 10^3$ TeV and $\alpha_e = 2$. The S spectra are shown by heavy lines, and the IC spectra are shown by thin lines. Although the main contribution to production of IC $\gamma$-rays is due to the 2.7-K MBR photons, in the calculations all other target photon fields are also taken into account, including diffuse galactic dust FIR with $w_{FIR} = 0.05$ eV cm$^{-3}$ ($T = 100$ K) and starlight NIR/optical radiation with $w_{sl} = 0.5$ eV cm$^{-3}$ ($T = 5000$ K). The synchrotron-self-Compton radiation is calculated assuming the size of the source $r_0 = 2$ pc. (b) As (a) except for the fixed value of the magnetic field $B = 10^{-5}$ G, and for three different exponential cut-offs: $E_0 = 100$ TeV (solid line), $E_0 = 10$ TeV (dashed line) and $E_0 = 1$ TeV (dot–dashed line). Note that, since all injection spectra are normalized to the same $L_e = 10^{37}$ erg s$^{-1}$, it results in some difference in the IC fluxes at low energies. (c) As (a) except for fixed values of the magnetic field $B = 10^{-5}$ G and $E_0 = 100$ TeV, and for four different ages of the pulsar (assuming stationary injection): $t_0 = 10^3$ yr (three-dot–dashed line), $t_0 = 10^4$ yr (solid line), $t_0 = 10^5$ yr (dashed line), $t_0 = 10^6$ yr (dot–dashed line).

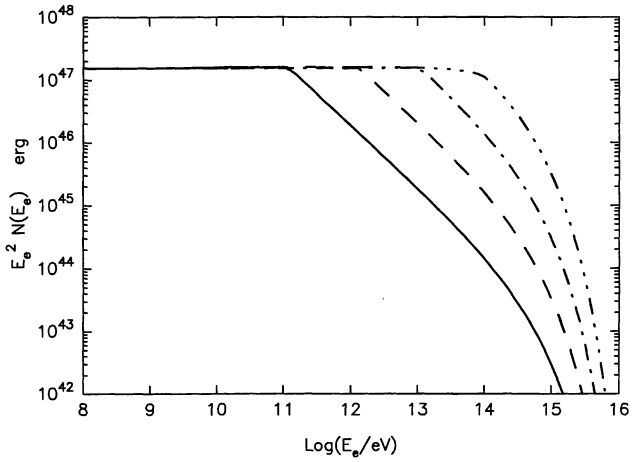


**Figure 4.** The spectra of relativistic electrons in the nebula for different magnetic fields: $B=10^{-4}$ G (solid lines), $B=3\times10^{-5}$ G (dashed lines), $B=10^{-5}$ G (dot–dashed lines) and $B=3\times10^{-6}$ G (three-dot–dashed lines). All other parameters are as in Fig. 3(a).

released in the synchrotron and IC channels are comparable.

Because of radiative cooling, the prompt spectrum of electrons above energies $E\geq E_*\simeq 12B_{-5}^{-2}(t_0/10^4\ \mathrm{yr})^{-1}$ TeV (defined from the condition $t_r=t_0$) becomes steeper, compared with the injection spectrum, by a factor of 1. An increase of the magnetic field leads to a decrease of the high-energy part of the electron spectrum, and correspondingly to suppression of the IC $\gamma$-ray luminosity above $E\sim h\nu(E_*/m_ec^2)^2$ as $L_\gamma\propto B^{-2}$. At the same time, since the synchrotron emissivity is proportional to $B^2$, the suppression of the number of high-energy electrons does not result in a reduction of the synchrotron luminosity. Moreover, since at $B\geq10^{-5}$ G the IC loss can be neglected, the synchrotron luminosity saturates at its maximum value (a factor of 2 higher than at $B=3\times10^{-6}$ G). A higher B-field has an impact on the low-frequency spectrum of the synchrotron radiation. Indeed, with the increase of the magnetic field, the modified ($\propto E_e^{-\alpha_e-1}$) part of the electron spectrum extends to lower energies, which eventually results in the transition of the radiation spectrum from $\epsilon^{-1.5}$ to $\epsilon^{-2}$.

On the other hand, higher magnetic fields lead to a shift of the spectrum of the synchrotron radiation to higher energies ($\epsilon\propto BE_e^2$). However, this cannot prevent the cut-off of radiation caused by the exponential cut-off in the injection spectrum of electrons. The corresponding cut-off is also seen in the spectrum of IC $\gamma$-rays. The impact of $E_0$, for the fixed value of the magnetic field $B=10^{-5}$ G, is demonstrated in Fig. 3(b). From this figure we may conclude that if the power-law spectrum of electrons continues beyond 10 TeV, the IC $\gamma$-ray luminosity peaks at TeV energies and synchrotron luminosity peaks at keV energies, with $L_\gamma/L_X=w_{ph}/w_B\simeq0.1B_{-5}^{-2}$. Thus, the X-ray fluxes may serve as an important indicator for the level of TeV $\gamma$-ray fluxes. The X-ray fluxes are dramatically suppressed if $E_0$ is less than 10 TeV. In particular, at $E_0\leq1$ TeV the X-rays disappear from the synchrotron spectrum (Fig. 3b). This leads also to strong suppression of TeV $\gamma$-ray fluxes. However, fluxes above 100 GeV still remain at a rather high level, $f(\geq100$ GeV$)\sim3\times10^{-12}$ erg cm$^{-2}$s$^{-1}$, which should be detectable for future atmospheric Cherenkov telescopes with a 100-GeV threshold energy. Thus, in such cases it is quite possible to expect VHE $\gamma$-ray nebulae surrounding pulsars *without* accompanying X-ray nebulae.

Since, in the case of the continuous injection of electrons, the energy $E_*\propto(B^2t_0)^{-1}$ is the only parameter which determines the spectral shape of electrons, the spectrum of the IC radiation is an invariant to the product $B^2t_0$. Obviously, the spectrum of the synchrotron radiation has a more complicated dependence on $B$ and $t_0$. In particular, since the characteristic energy of synchrotron photons is proportional to the $BE_e^2$, the transition region from $\epsilon^{-1.5}$ to $\epsilon^{-2}$ occurs at photon energies defined by the combination $B^{-3}t^{-2}$. Meanwhile, the position of the exponential cut-off in the S spectrum increases linearly with $B$, but is independent of $t_0$.

Dependence of the S and IC radiation spectra on the age of the pulsar for given $B=3\times10^{-6}$ G, corresponding to the typical magnetic field in the ISM, is shown in Fig. 3(c). Generally, the spectra of both synchrotron and IC radiations can be subdivided into three regions.

(a) At energies below $\epsilon_1$ and $E_1$ defined by equations (3) and (4) for $E_e=E_*$, the differential spectra of both components are a power-law with an index $(\alpha_e+1)/2$ which reflects the fact that the parent electrons with $E_e<E_*$ do not suffer significant energy losses during the lifetime of the source.

(b) At higher energies of the photons, the radiation is produced by electrons with spectra steeper (due to radiative energy losses) by a factor of 1, compared with the injection spectrum, therefore in these regions both components have a power-law index $(\alpha_e+2)/2$ up to energies $\epsilon_2$ and $E_2$ defined by equations (3) and (4) at $E_e=E_0$.

(c) At energies above $\epsilon_2$ and $E_2$, the spectra of both S and IC components of radiation have an exponential form reflecting the existence of the exponential high-energy cut-off in the spectrum of the electrons.

Note that above energies $\epsilon_1$ and $E_1$, i.e. in the regions (b) and (c), the radiation is the result of the electrons in the high-energy domain ($E\geq E_*$) where the stationary spectrum is already established. Therefore the synchrotron and IC luminosities saturate at the maximum levels which are determined only by the injection power $L_e(\geq E_*)$ and its sharing (equal to $w_B/w_{ph}$) between two channels of radiation. Thus, the parameter $S_0=L_{37}/d_{kpc}^2$ may serve as a reasonable indicator of the expected photon fluxes.

The extended X-ray nebulae around pulsars with $t_0\geq10^3$ yr can be seen at the level of $f_x\geq10^{-12}$ erg cm$^{-2}$ s$^{-1}$ if the parameter $S_0\geq0.01$, provided that a noticeable part of the spin-down luminosity is transformed into the wind of relativistic electrons with spectra extending beyond 10 TeV. This conclusion is almost independent of the ambient magnetic field. We therefore infer that such X-ray nebulae are starting to be seen by current sensitive detectors like *ROSAT* and *ASCA*. The list of 30 pulsars with the highest values of the parameter $S_0$, shown in Table 1, indicates that most of these pulsars do indeed show extended X-ray nebulae. Although very likely, the synchrotron origin of unpulsed X-radiation detected from these pulsars needs additional confirmation. The crucial test for this hypothesis would be the detection of accompanying TeV IC $\gamma$-radiation from these objects. In the next section, we will argue that the

recent reports on unpulsed X-ray and TeV $\gamma$-ray photons from the direction of PSR B1706 – 44 may imply the discovery of the first representative of the class of isolated pulsars surrounded by X-ray and $\gamma$-ray haloes.

## 4 SYNCHROTRON AND IC NEBULAE AROUND PSR B1706 – 44

The PSR B1706 – 44 is one of the seven radio pulsars detected by EGRET in $\gamma$-rays above 100 MeV (Thompson et al. 1996). Adopting the distance to the source of about $d = 1.8$ kpc (Taylor & Cordes 1993), and assuming that the radiation is beamed into one steradian, the luminosity of pulsed $\gamma$-radiation is estimated as $L_{\rm puls}(\geq 100\ {\rm MeV}) \simeq 3 \times 10^{34}$ erg s$^{-1}$. The *ROSAT* observations of this source revealed only unpulsed X-ray flux, with a $2\sigma$ upper limit on the pulsed fraction of 18 per cent (Becker, Brazier & Trümper 1995). The X-ray source can be extended with an angular size roughly of the instrument point spread function ( 1 arcmin), and is attributed to the synchrotron nebula (Becker et al. 1995). The soft X-ray emission in the range 0.1–2.4 keV, corrected for absorption, can be fitted by a power-law spectrum with a differential photon index $\alpha_{\rm x} = 2.4 \pm 0.6$ with the flux $f_{\rm x} \sim 3.2 \times 10^{-12}$ erg s$^{-1}$ (Becker et al. 1995). The corresponding luminosity $L_{\rm X} \approx 1.2 \times 10^{33}$ erg s$^{-1}$, which is only $\simeq 0.03$ per cent of the spin-down luminosity of the pulsar, $L_0 = 3.4 \times 10^{36}$ erg s$^{-1}$.

Recent observations of PSR B1706 – 44 in VHE $\gamma$-rays by the imaging Cherenkov telescope of the CANGAROO collaboration (Collaboration between Australia and Nippon for a Gamma-Ray Observatory in the Outback) have revealed unpulsed TeV radiation at a high confidence level (Kifune et al. 1995). Recently $\gamma$-radiation above 200 GeV from this object has also been detected by the Durham group (Turver, private communication). Although the possibility that this radiation represents the unpulsed component of the pulsar itself (see e.g. Cheng 1994) cannot be excluded, we present in this paper a view on the interpretation of the origin of this radiation which is more plausible, that is, that the $\gamma$-ray nebula is the result of IC scattering of the electrons injected by the pulsar into the surrounding ISM of low magnetic field.

The angular size of the $\gamma$-ray source does not exceed 0.1 deg (Kifune et al. 1995), which corresponds to a size for the $\gamma$-ray production region of $R \leq 3$ pc for the distance 1.8 kpc to the source. The detected $\gamma$-ray flux $I(\geq 1\ {\rm TeV}) \simeq 8 \times 10^{-12}$ cm$^{-2}$ s$^{-1}$. The absence of information on the $\gamma$-ray spectrum introduces an uncertainty, by a factor of 2, in the estimation of the VHE luminosity. In particular, assuming a power-law differential spectrum with index $\alpha_\gamma$, one obtains $L_\gamma(\geq 1\ {\rm TeV}) \simeq 4.7 \times 10^{33} A_\alpha$ erg s$^{-1}$ where $A_\alpha = (\alpha_\gamma - 1)/(\alpha_\gamma - 2)$ (for $\alpha_{\rm e} > 2$). In the framework of the hypothesis of the synchrotron origin of the X-ray nebula around PSR B1706 – 44 produced by the power-law spectrum of VHE electrons, the spectrum of the IC $\gamma$-rays should have a power-law distribution with the same index as the X-ray spectrum, thus $\alpha_\gamma = \alpha_{\rm x} \simeq 2.4$. Then $A_\gamma \simeq 3.5$, and correspondingly $L_\gamma(\geq 1\ {\rm TeV}) \simeq 1.6 \times 10^{34}$ erg s$^{-1}$. This exceeds by one order of magnitude the luminosity in the X-rays. At first glance this contradicts the balance between X-ray and $\gamma$-ray luminosities, since even for the lowest expected ISM magnetic field of about $3 \times 10^{-6}$ G, the ratio $w_{\rm B}/w_{\rm MBR} \simeq 1$, and thus $L_{\rm S} \simeq L_{\rm IC}$ (see equation 6). However, it should be stressed that equation (6) implies the $L_{\rm S}/L_{\rm IC}$ ratio in the appropriate energy bands of synchrotron and IC radiations connected with each other by equation (5). As follows from equations (3) and (4), the typical energies of electrons producing $\geq 0.1$ keV synchrotron photons in the magnetic field $3 \times 10^{-6}$ G and $\geq 1$ TeV IC $\gamma$-rays on the 2.7-K MBR are $\geq 41$ and $\geq 18$ TeV, respectively. Thus, assuming that the spectrum of electrons sharply steepens in this gap, one may significantly increase the ratio $L_{\rm IC}(\geq 1$ TeV$)/L_{\rm S}(\geq 0.1$ keV). Besides, the flux of the TeV IC $\gamma$-rays can be increased assuming the existence of an additional strong internal field of FIR radiation in the $\gamma$-ray production region. And finally, one should expect significant deviation of the S/IC flux ratio predicted by equation (6), if the observed fluxes of these two components of non-thermal radiation are produced in regions with essentially different angular sizes. We discuss these three possible scenarios in detail in the following.

### 4.1 Necessity of a sharp cut-off in the electron spectrum at $E_{\rm e} \ll 100$ TeV

In order to demonstrate that this idea is able to explain the observed fluxes of both X-rays and TeV $\gamma$-rays, in Fig. 5 we present the differential fluxes [in terms of $E^2 \times I(E)$], which

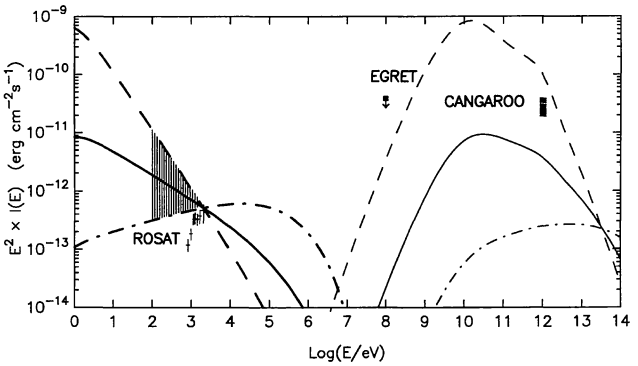


**Figure 5.** The nebular synchrotron (heavy lines) and IC (thin lines) radiation fluxes calculated for PSR B1706 – 44, assuming formally that the *prompt* spectrum of electrons, $N(E_{\rm e})$, is in the form of equation (11). The curves shown by the solid, dashed, and dot–dashed lines are for different values of the power-law index, $\alpha_{\rm e} = 3.8$, 2.6 and 5.0 respectively. Below $E_{\rm c} = 1$ TeV, the spectral cut-off with $\alpha_0 = 2$ is supposed (see equation 11), and the exponential cut-off energy $E_0 = 10^3$ TeV. The minimum possible magnetic field $B = 3 \times 10^{-6}$ G is assumed. The calculated spectra are normalized to the flux observed at 2 keV where the X-ray absorption is supposed to be negligible. The measured X-ray fluxes observed by *ROSAT* (crosses), as well as the range of the source X-ray fluxes corrected for absorption (dashed region) are shown (Becker et al. 1995). The integral fluxes of $\gamma$-rays corresponding to the calculated curves are: $I(\geq 1\ {\rm TeV}) = 1.5 \times 10^{-13}$, $1.2 \times 10^{-12}$ and $1.9 \times 10^{-11}$ photon cm$^{-2}$ s$^{-1}$ for $\alpha_{\rm e} = 2.6$, 3.8 and 5.0, respectively. The horizontally hatched region shows the range of differential fluxes at $E = 1$ TeV coresponding to the measured integral flux $I(\geq 1$ TeV$) \simeq 8 \times 10^{-12}$ photon cm$^{-2}$ s$^{-1}$ (Kifune et al. 1995), and is calculated assuming power-law index $\alpha_\gamma$ in the range 2.5–4 for the differential flux $I(E) \propto E^{-\alpha_\gamma}$. The upper limit of the EGRET for the unpulsed radiation above 100 MeV from PSR B1706 – 44 (Thompson et al. 1996) is also shown.

are calculated by formally assuming three different power-law indices $\alpha_e = 2\alpha_x - 1$ for the *prompt* spectra of electrons chosen so as to fit the range of the *ROSAT* X-ray fluxes (corrected for absorption): $\alpha_e = 2.6$ (dot–dashed curve), 3.8 (solid curve) and 5 (dashed curve). Besides, the exponential cut-off energy $E_0$ is taken high enough ($E_0 = 10^3$ TeV) to exclude its impact on the soft X-ray spectra. At the same time the low-energy cut-off $E_c = 1$ TeV allows us to avoid an unreasonably high requirement to the energetics in the electrons. The total energy in prompt electrons is determined from the normalization of the calculated X-ray fluxes to the observed one at 2 keV, where the absorption becomes negligible.

As is seen from Fig. 5, the observed X-ray and TeV $\gamma$-ray fluxes can be marginally explained only by assuming an extremely soft prompt electron spectrum with $\alpha_e = 5$. Note, however, that such extraordinarily steep power-law spectra, which require an injection spectrum as steep as $E_e^{-4}$, present an interest only for the purpose of a simple demonstration. In reality, such a steep spectrum may reflect the shape of the injection spectrum in the region corresponding to the maximum energies of the electron acceleration. Although the exact shape of the highest energy tail of the acceleration spectrum is rather unknown, it seems quite reasonable to approximate this part of the spectrum by an exponential cut-off as in equation (11).

In Fig. 6 we present S and IC radiation fluxes produced in the vicinity of PSR B1706 – 44 assuming continuous injection of the electrons during the lifetime of the pulsar $t = 1.7 \times 10^4$ yr, with a constant rate $L_e$ which is determined from the condition to provide the observed *ROSAT* X-ray flux at 2 keV. The electron injection spectrum is assumed in the form of equation (11) with $\alpha_e = 2$, $E_c = 1$ TeV, and three different values for $E_0 = 10$, 20, 30 TeV. The comparison of the calculated radiation spectra with observed fluxes shows

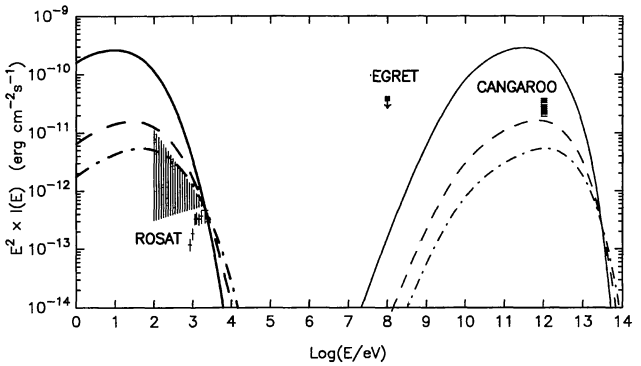


**Figure 6.** The S and IC radiation fluxes produced in the vicinity of PSR B1704 – 44, calculated for the magnetic field in the X-ray production region $B = 3 \times 10^{-6}$ G, assuming three different values for the exponential cut-off energy $E_0$ in equation (11): $E_0 = 10$ TeV (solid line), 20 TeV (dashed line and 30 TeV (dot–dashed line). Other parameters of the injection spectrum are $E_c = 1$ TeV, $\alpha_e = 2$, $\alpha_0 = -2$. The injection rate in relativistic electrons (which practically is at energies $E_e \geq E_c$) required to provide the observed X-ray flux at 2 keV is: $L_e = 7.3 \times 10^{36}$ erg s$^{-1}$ for $E_0 = 10$ TeV, $L_e = 3.4 \times 10^{35}$ erg s$^{-1}$ for $E_0 = 20$ TeV and $L_e = 1.1 \times 10^{35}$ erg s$^{-1}$ for $E_0 = 30$ TeV. The calculated integral IC $\gamma$-ray fluxes are $I(\geq 1$ TeV$) = 7.6 \times 10^{-11}$, $6.8 \times 10^{-12}$ and $2.5 \times 10^{-12}$ photon cm$^{-2}$ s$^{-1}$, respectively.

that it is impossible to explain simultaneously the X-ray and $\gamma$-ray fluxes, unless $E_0 \simeq 20$ TeV when the agreement between calculated and observed fluxes can be marginally accepted in both X-ray and TeV $\gamma$-ray energy regions. This result can be understood if one takes into account that the absolute number of electrons is determined by the normalization of the calculated synchrotron flux to the one observed at 2 keV. From equation (3) it follows that for the production of 2-keV synchrotron photons, electrons with energy

$$E_e \geq E_e^{(x)} \simeq 180 \left( \frac{B}{3 \times 10^{-6}\,\mathrm{G}} \right)^{-0.5} \left( \frac{\epsilon}{2\ \mathrm{keV}} \right) \mathrm{TeV} \qquad (13)$$

are required. Thus the parameter $g = E_e^{(x)}/E_0$ defines the suppression of the production of keV photons by a factor of $\exp(-g)$. The calculations show that the predicted synchrotron spectra agree with the *ROSAT* measurements if $g \geq 10$.

Meanwhile, 1-TeV $\gamma$-rays produced on the 2.7-K MBR require electrons with energy

$$E_e \geq E_e^{(\gamma)} \simeq 18\ \mathrm{TeV}. \qquad (14)$$

Thus an assumption of $E_0 \sim 20$ TeV which strongly suppresses the synchrotron radiation flux at 2 keV still does not dramatically reduce the flux of $E_\gamma \sim 1$ TeV IC $\gamma$-rays. However, a further decrease of $E_0$ cannot be accepted since, for the given normalization at 2 keV, it predicts fluxes of $\epsilon < 1$ keV X-rays significantly exceeding the observed fluxes. Besides, the values of $E_0 < 20$ TeV result in a strong increase of the required power in accelerated electrons. For example, in the case of $E_0 = 10$ TeV the required $L_e = 7.3 \times 10^{36}$ erg s$^{-1}$ exceeds the spin-down luminosity of the pulsar by a factor of 2.

On the other hand, the increase of $E_0$ above 20 TeV gives better agreement with the X-ray data, but cannot provide the observed TeV $\gamma$-ray fluxes. It should be noted, however, that this conclusion is relevant to the magnetic field $B \geq 3 \times 10^{-6}$ G. One may soften the constraint on $E_0$ by formally assuming a lower magnetic field. For example, in the case of $B = 10^{-6}$ G, the energy $E_e^{(x)} \sim 300$ TeV, thus the condition of $g \leq 10$ requires $E_0 \geq 30$ TeV. Note that large values of $E_0 \gg 10$ TeV essentially increase the efficiency of the TeV $\gamma$-ray production. Besides, lower magnetic fields change the sharing of electron energy losses in favour of the IC process. Thus we should expect essentially better agreement of the calculation with the observed X-ray and TeV $\gamma$-ray data if the magnetic field in the vicinity of this specific pulsar were significantly lower than the average field of the ISM. In Fig. 7 we show the dependence of the X-ray and $\gamma$-ray fluxes on magnetic field for $E_0 = 50$ TeV. We see that an agreement of flux predictions in X-ray and $\gamma$-ray channels can be reached only at $B \leq 10^{-6}$ G.

### 4.2 Enhanced field of FIR near the pulsar

Another principal possibility for increasing the flux of IC $\gamma$-rays, but keeping the magnetic field at the level of the ISM, is to assume the existence of an enhanced radiation of FIR in the 1 pc vicinity of the pulsar. In Fig. 8 the solid curves are calculated assuming that there is no additional source of FIR except for the diffuse interstellar background

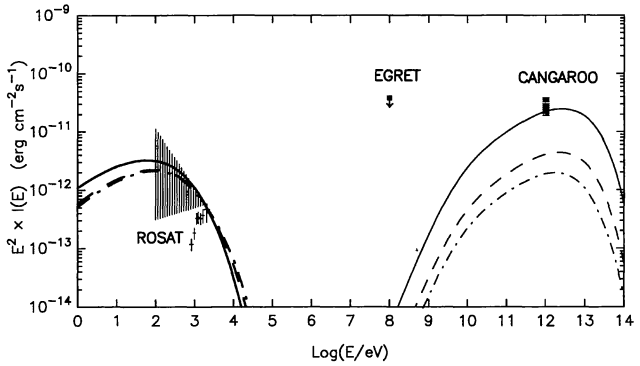


**Figure 7.** As Fig. 6, but in the case of fixed energy $E_0=50$ TeV, and different magnetic fields in the X-ray production region: $B=1\times10^{-6}$ G (solid lines), $B=2\times10^{-6}$ G (dashed lines) and $B=3\times10^{-6}$ G (dot–dashed lines). The calculated IC $\gamma$-ray fluxes are $I(\geq1\ \mathrm{TeV})=1.4\times10^{-11}$, $2.4\times10^{-12}$, $1\times10^{-12}$ photon cm$^{-2}$ s$^{-1}$, and the required luminosities in the relativistic electrons are $L_e=4.3\times10^{35}$, $8.1\times10^{34}$ and $3.9\times10^{35}$ erg s$^{-1}$, respectively.

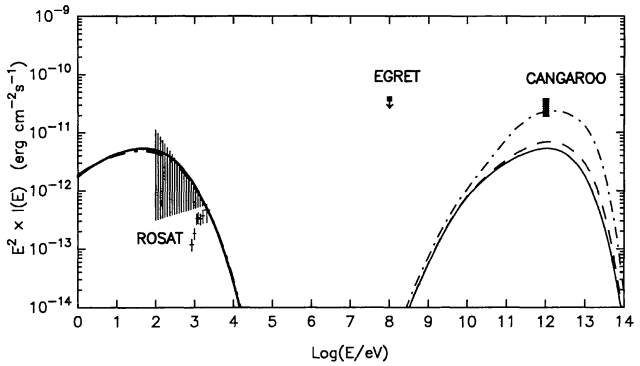


**Figure 8.** The fluxes of the S and IC radiations, produced in the X-ray nebula surrounding PSR B1706 − 44, calculated for the fixed magnetic field $B=3\times10^{-6}$ G, but assuming different values for the energy density of the FIR photons with $T=100$ K in the X-ray nebula: $w_{\rm FIR}=0.05$ eV cm$^{-3}$ (solid line), $w_{\rm FIR}=0.5$ eV cm$^{-3}$ (dashed line) and $w_{\rm FIR}=5$ eV cm$^{-3}$ (dot–dashed line). The parameters of the electron injection spectrum are the same as in Fig. 6 with $E_0=30$ TeV. The calculated integral $\gamma$-ray fluxes are $I(\geq1$ TeV$)=2.5\times10^{-12}$, $3.5\times10^{-12}$ and $1.3\times10^{-11}$ photon cm$^{-2}$ s$^{-1}$. The injection rates in relativistic electrons are $L_e=1.1\times10^{35}$, $1.2\times10^{35}$ and $1.4\times10^{35}$ erg s$^{-1}$, respectively.

radiation with dust temperature 100 K and energy density $w_{\rm FIR}\simeq0.05$ eV cm$^{-3}$. The dashed and dot–dashed curves correspond to the enhanced FIR radiation density $w_{\rm FIR}=0.5$ and 5 TeV cm$^{-3}$, respectively. Although the assumption of 100-fold enhancement of the FIR relative to the diffuse galactic background level can explain both the X-ray and $\gamma$-ray fluxes, it seems difficult to justify the origin of such an intense field which exceeds by a factor of 10 even the dust FIR density of the Crab. Since the angular size of the X-ray nebula is estimated to be about that of the *ROSAT* point spread function (Becker et al. 1995), the spatial size of the source is estimated to be of about $r\simeq0.3$ pc, assuming $d\simeq1.8$ kpc and angular radius of the source $\sim0.5$ arcmin. The luminosity of the FIR source then required to provide 5 eV cm$^{-3}$ photon density in the X-ray nebula is $L_{\rm FIR}=4\pi r^2 c w_{\rm FIR}\simeq3\times10^{36}$ erg s$^{-1}$. We are not aware of the existence of such source, although this could easily be checked by the *Infrared Space Observatory* (*ISO*).

### 4.3 Production of IC $\gamma$-rays outside of the compact X-ray nebula

The ways in which to match the observed X-ray and $\gamma$-ray fluxes discussed above require rather specific conditions in the production region: magnetic field lower, by a factor of $\sim3$, than the ISM magnetic field and/or internal FIR photon field by 2 orders of magnitude exceeding the diffuse galactic background. However, these very tight requirements can essentially be softened if one assumes that the flux of TeV $\gamma$-rays detected by CANGAROO is produced in a region significantly larger than the rather compact X-ray nebula detected by *ROSAT*.

Indeed, in previous sections we have assumed a priori that the X-ray and $\gamma$-ray fluxes are produced in the same region. In fact, the angular size of the region in which the TeV $\gamma$-ray flux originates could be significantly larger than the size of the X-ray nebula measured by *ROSAT*. The upper limit to the angular size of the TeV $\gamma$-ray source, which is estimated to be about 0°.1 (Kifune et al. 1995), is still too large to conclude that the X-rays and $\gamma$-rays are produced in the same region. Therefore we assume that the size of the $\gamma$-ray nebula exceeds 1 arcmin. If so, the number of electrons responsible for the observed X-ray flux may be significantly less than the total number of electrons which occupy the larger space. In this case, the reason why we see only compact X-ray nebulae could be due to the increase of the magnetic field from $B\sim B_{\rm ISM}$ to significantly higher values in the neighbourhood of the pulsar (e.g. at $r\leq1$ pc). Note that in this approach, the constraint on the value of the magnetic field in the X-ray nebula (which is crucial if one assumes that the observed X-ray and $\gamma$-ray fluxes are produced in the same region) is no longer based on the simple condition of the synchrotron/IC sharing of the energy losses of electrons, but has a more complicated dependence on the model parameters. The main condition we are now concerned with is that the greater part of the $\geq10$ keV electrons escape the X-ray nebula without significant losses. Thus the electron escape time from the X-ray nebula is one of the important model parameters in this approach. Generally the escape time is a function of energy, and we use a power-law function $\tau(E_e)=\tau_{20}(E_e/20\ \mathrm{TeV})^{-\delta}$. Since for us the 20-TeV electrons producing 1-TeV IC photons present the prime interest, we normalize the escape time to the value $\tau_{20}$ at energy $E_e=20$ TeV.

In Fig. 9(a) we present the results of flux calculations (using equation 10), assuming the following approximation for the magnetic field: $B=B_x=3\times10^{-5}$ G inside of the X-ray nebula ($r\leq0.3$ pc), and $B=B_\gamma=3\times10^{-6}$ G outside. For the escape time $\tau$ we take $\delta=0.5$, and three different values for $\tau_{20}$: $\tau_{20}=5$ (solid curves), 10 (dashed curves) and 20 yr (dot–dashed curves). The fluxes produced in the X-ray nebula are shown by heavy lines (the *ROSAT* data should be compared with these curves), and the fluxes produced outside of this region are shown by thin lines (the CANGAROO flux should be compared with the sum of the thin and heavy curves).

In Fig. (b) we fix the escape time ($\delta=0.5$ and $\tau_{20}=10$ yr), but allow $B_x$ to vary within $(2–5)\times10^{-5}$ G. From Figs 9(a)

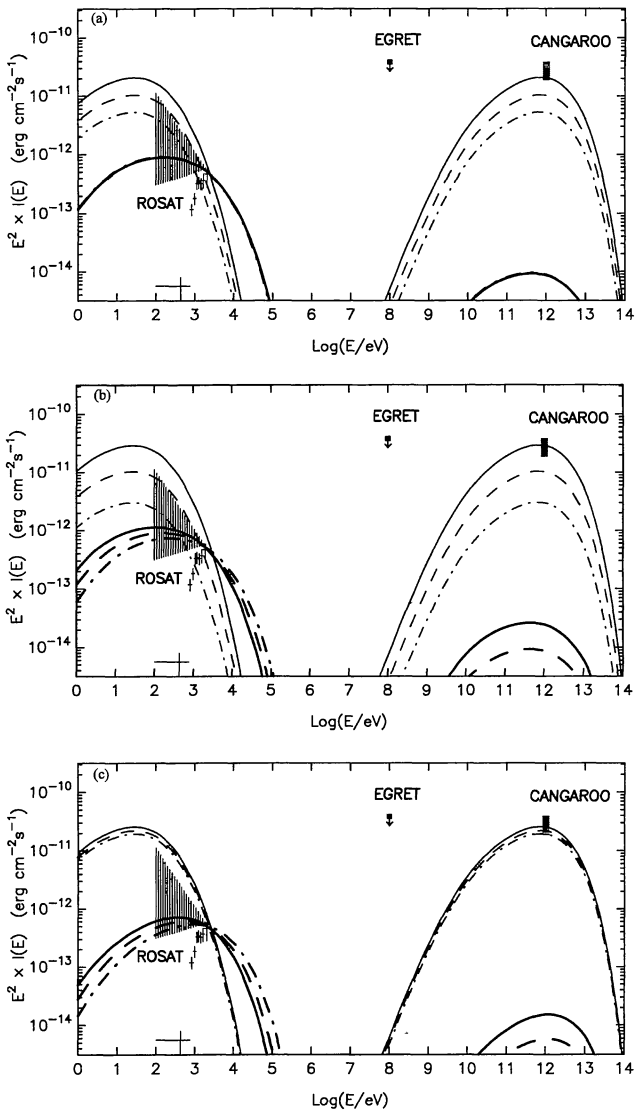


**Figure 9.** (a) The S and IC radiation fluxes produced in the vicinity of PSR B1706 − 44 in two regions with different sizes $r_x \leq 0.3$ pc and $r_\gamma \leq 3$ pc, calculated for the magnetic fields $B = B_x = 3 \times 10^{-5}$ G and $B = B_\gamma = 3 \times 10^{-6}$ G, respectively. The fluxes produced in the region $r \leq r_x$ are shown by heavy lines, and fluxes produced in the region $r_x \leq r \leq r_\gamma$ are shown by thin lines. Three different values of $\tau_{20}$ for the escape time of relativistic electrons from the compact region with high B-field (i.e. from the X-ray nebula) into the surrounding region with smaller B-field are assumed: $\tau_{20} = 5$ yr (solid lines), 10 yr (dashed lines) and 20 yr (dot–dashed lines). The escape time is taken to be energy-dependent, with the power-law index $\delta = 0.5$. Parameters of the electron injection spectrum in equation (11) are $E_0 = 20$ TeV, $E_c = 1$ TeV, $\alpha_e = 2$, $\alpha_0 = -2$. The calculated electron injection rates and the IC $\gamma$-ray fluxes are: $L_e = 4.5 \times 10^{35}$ erg s$^{-1}$ and $I(\geq 1\ \text{TeV}) = 9 \times 10^{-12}$ photon cm$^{-2}$ s$^{-1}$ for $\tau_{20} = 10$ yr; $L_e = 1.2 \times 10^{35}$ erg s$^{-1}$ and $I(\geq 1\ \text{TeV}) = 2.3 \times 10^{-12}$ photon cm$^{-2}$ s$^{-1}$ for $\tau_{20} = 20$ yr. (b) As (a) for the fixed value of $\tau_{20} = 10$ yr and three different values of the magnetic field in the compact X-ray nebula: $B_x = 2 \times 10^{-5}$ G (solid lines), $B_x = 3 \times 10^{-5}$ G (dashed lines) and $B_x = 5 \times 10^{-5}$ G (dot–dashed lines). The calculated IC $\gamma$-ray fluxes are $I(\geq 1\ \text{TeV}) = 1.3 \times 10^{-11}$ photon cm$^{-2}$ s$^{-1}$, $I(\geq 1\ \text{TeV}) = 4.5 \times 10^{-12}$ photon cm$^{-2}$ s$^{-1}$ and $I(\geq 1\ \text{TeV}) = 1.3 \times 10^{-12}$ photon cm$^{-2}$ s$^{-1}$. (c) As (a) in the case of energy-independent escape, $\delta = 0$, and three different combinations of $B_x$ and $\tau_{20}$ chosen so that the parameter $C_0 = B_x^2 \times \tau_{20} = 3.5 \times 10^{-9}$ G$^2$ yr: $B_x = 2 \times 10^{-5}$ G and $\tau_{20} = 8.75$ yr (solid lines); $B_x = 3 \times 10^{-5}$ G and $\tau_{20} = 3.9$ yr (dashed lines); and $B_x = 5 \times 10^{-5}$ G and $\tau_{20} = 1.4$ yr (dot–dashed lines). The calculated integral IC $\gamma$-ray fluxes are $I(\geq 1\ \text{TeV}) = 1.1 \times 10^{-11}$ photon cm$^{-2}$ s$^{-1}$, $I(\geq 1\ \text{TeV}) = 9.5 \times 10^{-12}$ photon cm$^{-2}$ s$^{-1}$ and $I(\geq 1\ \text{TeV}) = 8.4 \times 10^{-12}$ photon cm$^{-2}$ s$^{-1}$. In all three cases the luminosity in relativistic electrons which is required to provide the observed X-ray flux at 2 keV is $L_e \sim 5 \times 10^{35}$ erg s$^{-1}$.

and (b) it follows that for some combination of the parameters $B_x$ and $\tau_{20}$, it is easily possible to match the *ROSAT* and CANGAROO fluxes. The principal parameter which defines the fraction of the injected electrons ($\geq 10$ TeV) escaping the X-ray nebula is the ratio of the escape time to the synchrotron cooling time, $\tau/t_S \propto B_x^2 \times \tau_{20}$. In Fig. 9(c) we show the calculated fluxes of synchrotron and IC photons for three different combinations of $B_x$ and $\tau_{20}$, chosen so that the parameter $C_0 = B_x^2 \times \tau_{20}$ is fixed at a constant value of $3.5 \times 10^{-9}$ G$^2$ yr. It should be noted that this value of $C_0$, which allows us to explain the X-ray and $\gamma$-ray fluxes (see Fig. 9c), is obtained for a given cut-off energy $E_0 = 20$ TeV. The increase of $E_0$ requires somewhat smaller values of $C_0$. On the other hand, larger values of $C_0$ may be excluded because they would require a cut-off in the electron injection spectrum significantly below $E_0 = 20$ TeV, which results in a too low efficiency of $\geq 1$ TeV $\gamma$-ray production.

Assuming that electrons propagate in the nebula rectilinearly with the speed of light, the electron escape time $\tau_{20}$ is $\sim 1$ yr, and thus the required magnetic field $B_x$ is estimated as $B_x = (C_0/\tau_{20})^{1/2} \simeq 6 \times 10^{-5}$ G. In fact this value of $B_x$ should be considered as an upper limit since the bulk motion of electrons could be significantly slower than the speed of light, for example due to convection or diffusion in the X-ray nebula. For example, for $B = 2 \times 10^{-5}$ G the escape time is of the order of about 10 yr, which corresponds to the effective speed of propagation of $\geq 20$ TeV electrons $v_{\text{eff}} \sim 0.1c$ in scales $\leq 0.3$ pc. At larger distances from the pulsar, the speed of the propagation of electrons seems to be slowed down. Indeed, the assumption that the bulk of electrons, produced during $\sim 10^4$ yr and responsible for the observed TeV fluxes, are still effectively captured in the radius $r_\gamma \leq 3$ pc, which corresponds to the angular size of the $\gamma$-ray source $\leq 0.1°$, requires the speed of propagation $v_{\text{eff}}$ to be $\sim 10^{-3}c$. The decrease of $v_{\text{eff}}$ with distance $r$ is perhaps the result of the magnetohydrodynamical (rather than diffusive) character of the propagation of electrons. Such behaviour of $v_{\text{eff}}$ is in agreement with the MHD model of Kennel & Coroniti (1984) developed for the Crab Nebula.

## 5 DISCUSSION

The discovery of the X-ray nebulae around many radio pulsars opens an interesting prospect for future VHE $\gamma$-ray observations by atmospheric Cherenkov telescopes. Indeed, if these X-ray nebulae really are of the synchrotron origin, it would unambiguously imply the existence of the accompanying $\gamma$-ray nebulae produced due to IC scattering of the relativistic electrons on the 2.7-K MBR.

The TeV fluxes can easily be estimated assuming that the $\gamma$-rays are produced in the X-ray nebula. For a given magnetic field, the expected energy fluxes of TeV $\gamma$-rays are directly connected with the observed X-ray fluxes by equation (6) at photon energies given by equation (5). Since the

target for production of the IC $\gamma$-rays is known, 2.7-K MBR, the only unknown parameter for such an estimate is the ambient magnetic field $B$. The sharing of the energy fluxes between synchrotron X-rays and IC $\gamma$-rays is determined by the ratio $(B^2/8\pi)/w_{\rm MBR} \simeq 1(B/3\times10^{-6}\,{\rm G})^2$. The energy fluxes of many X-ray nebulae presented in Table 1 are between $10^{-12}$ and $10^{-11}$ erg cm$^{-2}$ s$^{-1}$. Therefore, the flux sensitivity of the atmospheric imaging Cherenkov telescopes, $10^{-12}$ erg cm$^{-2}$ s$^{-1}$, which most likely will be reached in the near future, would allow us to detect many representatives of this new class of galactic non-thermal objects in VHE $\gamma$-rays, if the magnetic field in the $\leq 1$ pc vicinity of the pulsar were as low as the interstellar magnetic field $B_{\rm ISM} \sim (3\text{–}5)\times10^{-6}$ G. At the same time the fluxes of GeV $\gamma$-rays under even the most optimistic assumptions appears to be significantly below that of the EGRET sensitivity.

It should be admitted, however, that the assumption about a low magnetic field close to the pulsar is rather speculative, and cannot easily be justified. Note, in particular, that the magnetic field in the sub-parsec scale is likely produced by the magnetized electron–positron wind. In the case of the Crab pulsar, the nebular magnetic field $B \geq 10^{-4}$ G is generated by such a wind (Kennel & Coroniti 1984). In the case of less powerful pulsars, the nebular magnetic field should be smaller; however, it is not likely to be much less than $10^{-5}$ G. If so, one might conclude that the one should expect VHE $\gamma$-ray fluxes below $10^{-12}$ erg cm$^{-2}$ s$^{-1}$. Even very extreme assumptions about possible targets for IC $\gamma$-ray production, in the form of FIR photons, with density exceeding by two orders of magnitude the diffuse FIR background, cannot easily change such a pessimistic view. This might serve as an argument in favour of the origin of the TeV emission being an unpulsed radiation of the pulsar itself (Cheung & Cheng 1994; Bogovalov & Kotov 1995). However, we argue that it is premature to abandon the hypothesis of the IC origin of TeV $\gamma$-rays observed from PSR B1706 – 44, if assuming that the production of $\gamma$-rays takes place on spatial scales essentially larger than the observed compact X-ray nebula.

Indeed, if the $\geq 10$ TeV electrons quickly leave the compact X-ray nebula (with high magnetic field) without significant synchrotron energy loss, then we see only the small (and bright) part of the X-ray nebula. Meanwhile, since the target photon field (2.7-K MBR) for the production of the IC $\gamma$-rays is spatially homogeneous, the size of the *detectable* IC $\gamma$-ray nebula should exceed the size of the *visible* X-ray nebula. In this case there is no longer a direct relation between the *observed* X-ray and $\gamma$-ray fluxes, in particular the predictions of $\gamma$-ray fluxes essentially depend on the model parameters such as spatial profile of the magnetic field within several parsecs from the pulsar, and on the speed of the propagation (escape) of electrons from the compact X-ray nebula. Fig. 9 clearly demonstrates that this approach can be successful. The observed size of the X-ray nebula of about 0.5 arcmin and of the TeV $\gamma$-ray source $\leq 0.1°$ does not exclude such a natural kind of interpretation of the X-ray and TeV $\gamma$-ray data.

At the same time, the hypothesis of the existence of the X-ray and TeV $\gamma$-ray haloes surrounding the pulsar PSR B1706 – 44 needs further observational confirmation. In particular new spectroscopic X-ray measurements of this nebula seem to be important, especially in the energy region 1–10 keV where the absorption does not significantly modify the source spectrum. Note that one should not necessarily expect 'standard' power-law spectra because the photons in this energy region are produced by the exponential tail of the spectrum of electrons. Therefore, the detection of an 'exponential type' X-ray spectrum in this energy region should not be considered an indication of the thermal origin of the radiation.

On the other hand, the synchrotron origin of the X-ray nebula can be supported by the discovery of non-thermal nebulae in lower frequency photons. The expected fluxes of non-thermal radiation in the broad-band region from GHz frequencies to 100 TeV $\gamma$-rays, calculated for different injection spectra and escape times of electrons, are shown in Fig. 10. The heavy lines correspond to synchrotron fluxes from the observed X-ray nebula region with angular radius 0.5 arcmin, and the thin lines are for the IC $\gamma$-ray fluxes expected from the more extended region $\leq 0.^\circ1$. Note that the energy losses of electrons at low energies ($\leq 1$ TeV) are negligible, thus they do not modify the injection spectrum. At the same time the electron spectrum in the X-ray nebula could be modified due to the energy-dependent escape, $\tau(E) = \tau_{20}(E/20\ {\rm TeV})^{-\delta}$. If the case of energy-independent propagation of electrons ($\delta = 0$), the differential fluxes of the synchrotron radiation below 100 eV and IC radiation below 100 GeV have a power-law index $\alpha_\gamma = (\alpha_e + 1)/2 = 1.5$ (solid lines in Fig. 10). In order to demonstrate the effect of the energy-dependent escape or steep injection spectrum of electrons on the radiation spectra at low energies, in Fig. 10 we also show the fluxes calculated for $\delta = 0.5$ for two power-law injection spectra of electrons with $\alpha_e = 2$ (dashed lines) and $\alpha_e = 2.5$ (three-dot–dashed lines). The differences of the fluxes becomes noticeable at near-infrared wavelengths and below, thus the detection of extended ($\leq 1$ arcmin) synchrotron radio and infrared haloes around the pulsar may give important information on the injection spectrum

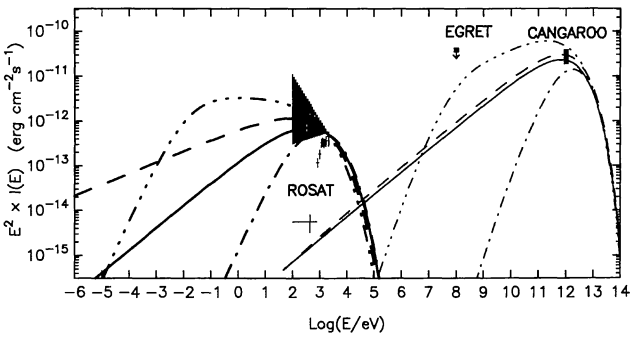


**Figure 10.** The expected fluxes of the broad-band synchrotron radiation produced in the region of the compact X-ray nebula around PSR B1706 – 44 with angular size $\theta_x \sim 0.5$ arcmin (heavy lines) and in the more extended IC $\gamma$-ray nebula with $\theta_\gamma \leq 0.^\circ1$ (thin lines). The magnetic field profile is approximated as $B_x = 2\times10^{-5}$ G and $B_\gamma = 3\times10^{-6}$ G inside and outside of the compact X-ray nebula. The escape time of electrons is given by $\tau(E_e) = 10(E/20\ {\rm TeV})^{-\delta}$ yr. The injection spectrum of electrons is given by equation (11) with $E_0 = 20$ TeV and $\alpha_0 = -2$. The solid curves are for $\alpha_e = 2$, $E_c = m_e c^2$, $\delta = 0$; dashed curves: $\alpha_e = 2$, $E_c m_e c^2$, $\delta = 0.5$; three-dot–dashed curves; $\alpha_e = 2.5$, $E_c = 100$ GeV, $\delta = 0.5$; the dot–dashed curves correspond to injection spectrum with $E_c = 10$ TeV and $\delta = 0.5$.

of electrons and the character of their propagation in the nebula.

The radiation fluxes in Fig. 10 calculated for single power-law injection spectra of electrons ($E_c = m_e c^2$) require the injection rate $L_e \simeq 5 \times 10^{36}$ erg s$^{-1}$ which slightly exceeds the spin-down luminosity of the pulsar PSR B1706 − 44. However, the energy requirement could be significantly softened if one assumed low-energy cut-off in the injection spectrum at $E_e \gg m_e c^2$. This, however, would result in suppression of the low-frequency synchrotron radiation down to the non-observable level. This is demonstrated in Fig. 10 by the heavy dot–dashed curve calculated assuming $E_c = E_0/2 = 10$ TeV. The spectrum formally given by equation (11) with $E_c$ and $E_0$ rather close to each other actually corresponds to a 'monoenergetic'-type distribution of electrons with the mean energy $\bar{E}_e \sim 15$ TeV and dispersion of $\Delta E_e \sim \bar{E}_e$. It is worthwhile to note that an injection spectrum of this kind cannot be considered as a formal and unrealistic one. In fact, the hypothesis of the relativistic magnetized wind from the pulsar almost automatically implies the production of a monoenergetic flux of electrons. The redistribution of these electrons to a power-law spectrum could occur later on the wind termination shock, which perhaps is the case with the Crab (e.g. Kennel & Coroniti 1984). However, for the less powerful pulsars the formation of the wind termination shocks may not be as effective as in the Crab. As a consequence, the spectrum of electrons injected into the nebula may be not significantly broadened. Thus the broad-band study of the synchrotron nebula may provide very important insight into the physics of the relativistic electron–positron winds in the pulsars.

Independently of the injection spectrum and the propagation of electrons at low energies ($\leq 10$ TeV), important information confirming the existence of the synchrotron X-ray nebulae around isolated pulsars can be provided by the detection of (more) extended TeV $\gamma$-ray haloes. Since the target for production of the IC $\gamma$-rays is the universal 2.7-K MBR, the information contained in the $\gamma$-ray observations is almost model-independent. Thus the search for TeV $\gamma$-ray haloes around pulsars with X-ray nebulae by existing or planned imaging atmospheric Cherenkov telescopes with sensitivities $\sim 10^{-12}$ erg cm$^{-2}$ s$^{-1}$ presents a great interest.

It is possible to estimate VHE $\gamma$-ray luminosities from the X-ray nebula listed in Table 1, by using the observed luminosity of X-ray and by taking the parameters discussed in the present paper, such as the strength of magnetic field, as being adequate for each object. Most of these X-ray nebulae have an angular size of less than 0.1 degree, which is the typical width of the point spread function of the current imaging Cherenkov technique. Thus, VHE $\gamma$-ray emisson from the same regions of the X-ray nebulae appears as though from a point-like source, implying that anticipated reduction of sensitivity on extended emission is not the case. The next generation of imaging atmospheric Cherenkov telescopes (IACTs) attempts to reach a sensitivity of $10^{-13}$ erg cm$^{-2}$ s$^{-1}$, and may allow us to probe VHE $\gamma$-ray luminosities down to the level of $10^{31}$ (d/1 kpc)$^2$ erg s$^{-1}$. Many of the objects in Table 1 could appear as VHE $\gamma$-ray sources.

Furthermore, if the electrons responsible for the synchrotron X-ray emission effectively escape the region of high magnetic field, the latter presumably being the reason why we see the X-ray nebulae, then the expected fluxes of $\gamma$-rays from more extended regions could be even higher than the X-ray fluxes, i.e. $10^{-11}$ erg cm$^{-2}$ s$^{-1}$, which may be the case with PSR B1706 − 44. With such enhancement in IC emission as compared with synchrotron X-rays, the extended $\gamma$-ray nebulae could become detectable, even if we take into account the fact that the sensitivity of the IACTs on extended emission over about 1° is, by a factor of 10, less than for point-like sources. It is interesting to note that some of the synchrotron X-ray nebulae, such as around the Vela pulsar, PSR B1951 + 32 (Safi-Harb, Ögelman & Finley 1995) and PSR B1823 − 13 (Finley, Srinivasan & Park 1996), do have a complex spatial structure. For example, PSR B1951 + 32, in addition to a point X-ray source (pulsar), has a compact ($\leq 1$ arcmin) nebula, a diffuse nebula, and a 'cone-like' feature of $\sim 1°$. Safi-Harb et al. (1995) estimated $B \sim 3.4 \times 10^{-6}$ G and the mean value of energy of electrons $E_e \sim 80$ TeV for the eastern diffuse nebula of 5 arcmin angular spread, by assuming equipartition between particle and energy density of the nebula. If so, one should expect the flux of VHE $\gamma$-rays at the level of $5 \times 10^{-12}$ erg cm$^{-2}$ s$^{-1}$ from this extended X-ray nebula which still could be considered as almost a point-like source for the IACTs. Note that in the proposed 'electron escape' scenario the X-ray spectra from the extended nebula should be steeper than in the compact nebula, due to two reasons, namely (1) radiative cooling of electrons at large distances from the pulsar, and (2) lower magnetic field. This effect is clearly seen in Fig. 9. Remarkably, the effect of steepening of the X-ray spectrum seems to be observed from the Vela, where the compact nebula with angular size $\leq 5$ arcmin is characterized by a differential power-law index $\simeq 1.7$, while in the extended nebula within 5–45 arcmin the index is 3.1 (Markwardt & Ögelman 1995). In the case of PSR B1951 + 32, the compact and diffuse nebulae have similar values of spectral index, 2.1 and 1.8 respectively (though with large errors of $\pm 0.2$ and $+0.5$–$0.8$, respectively), which might not appear very consistent with our expectation that the outer nebula should have a softer spectrum. However, when we go further to larger distances from the pulsar, the emission from the cone-like feature has a very steep spectrum with index $> 4$ when fitted with a power law (Safi-Harb et al. 1995). When we apply the 'electron escape' model to explain the 'multi-structure' of the X-ray nebulae, the data from the VHE $\gamma$-rays would add clues to clarify certain characteristics of the structure, such as the variation of magnetic field strength and the propagation of energetic electrons.

Finally, we would like to mention the recent discovery of X-ray nebulae around two nearby pulsars, Geminga and B1929 + 10. The observations of TeV $\gamma$-rays would undoubtedly confirm the non-thermal origin of the nebulae, and thus be direct evidence of the acceleration of VHE electrons in these sources. These objects are close enough to provide a non-negligible part of the observed TeV electrons (Nishimura et al. 1980), $\gamma$-ray emission giving strong evidence that Geminga is one of the sources of local high-energy electrons, as well as limiting the model parameters of propagation and confinement of electrons in the Galaxy (e.g. Aharonian, Atoyan & Völk 1995; Nishimura et al. 1995).

## ACKNOWLEDGMENTS

We are grateful to S. Shibata and N. Kawai for providing us with their *ASCA* X-ray results on pulsar-driven nebulae before publication. We also thank the referee, H. Ögelman, for useful comments. AMA is grateful to the Max-Planck-Institut für Kernphysik for hospitality during his visit to Heidelberg; his work was supported through the Verbundforschung Astronomie/Astrophysik of the German BMBF under grant No. 05-2HD66A(7).

## REFERENCES

Aharonian F. A., 1995, Nucl. Phys. B, 39A, 193
Aharonian F. A., Atoyan A. M., 1995, Astroparticle Phys., 3, 275
Aharonian F. A., Atoyan A. M., Völk H. J., 1994, A&A, 294, L41
Arons J., 1996, Space Sci. Rev., 75, 235
Atoyan A. M., Aharonian F. A., 1996, MNRAS, 278, 525
Becker W., Brazier K. T. S., Trümper J., 1995, A&A, 298, 528
Blumenthal G. R., Gould R. J., 1970, Rev. Mod. Phys., 42, 237
Bogovalov S. V., Kotov Yu. D., 1995, MNRAS, 262, 75
Chadwick P. M., McComb T. J. L., Turver K. E., 1990, J. Phys. G, 16, 1773
Cheng K. S., 1994, in Kifune T., ed., Proc. International Workshop, Towards a Major Atmospheric Cherenkov Detector II. Universal Academy Press, Tokyo, p. 25
Cheng K. S., Ho C., Ruderman M. A., 1986, ApJ, 300, 500
Cheung W. M., Cheng K. S., 1994, ApJS, 90, 827
Chi X., Cheng K. S., Young E. C., 1996, ApJ, 459, 83L
Daugherty J. K., Harding A. K., 1982, ApJ, 252, 337
de Jager O. C., 1996, in Cristi M., ed., Proc. International Workshop, Towards a Major Atmospheric Cherenkov Detector III. Univ. Padova, Padova, p. 452
de Jager O. C., Harding A. K., 1992, ApJ, 396, 161
Finley J. P., Srinivasan R., Park S., 1996, ApJ, 466, 938
Ginzburg V. L., 1979, Theoretical Physics and Astrophysics. Pergamon Press, Oxford
Ginzburg V. L., Syrovatskii S. I., 1964, The Origin of Cosmic Rays. Pergamon Press, Oxford
Harrus I. M., Hughs J. P., Helfand D. J., 1996, ApJ, 469, L161
Kawai N., Tamura K., 1996, in Johnston S., Walker M. A., Bailes M., eds, Proc. IAU Colloq. 160, Pulsars: Problems and Progress. Reidel, Dordrecht, p. 367
Kennel C. F., Coroniti F. V., 1984, ApJ, 283, 694
Kifune T., 1996a, in Johnston S., Walker M. A., Bailes M., eds, Proc. IAU Colloq. 160, Pulsars: Problems and Progress. Reidel, Dordrecht, p. 339
Kifune T., 1996b, Space Sci. Rev., 75, 31
Kifune T. et al., 1995, ApJ, 438, L91
Markwardt C. B., Ögelman H., 1995, Nat, 375, 40
Marsden P. L., Gillett F. C., Jennings R. E., Emerson J. P., De Jong T., Olnon F. M., 1984, ApJ, 278, L29
Mathis J. S., Mezger P. G., Panagia N., 1983, A&A, 128, 212
Nishimura J. et al., 1980, ApJ, 238, 394
Nishimura J., Kobayashi T., Komori Y., Tateyama N., 1995, Proc. 24th Int. Cosmic Ray Conf., 3, 29
Nolan P. L. et al., 1996, A&AS, 120, p. 61
Ramanamurthy P. V., Fichtel C. E., Kniffen D. A., Sreekumar P., Thompson D. J., 1996, ApJ, 458, 755
Safi-Harb S., Ögelman H., Finley J. P., 1995, ApJ, 439, 722
Tamura K., Kawai N., Yoshida A., Brinkmann W., 1996, PASJ, 48, L33
Taylor J. H., Cordes J. M., 1993, ApJ, 411, 674
Taylor J. H., Manchester R. N., Lyne A. G., 1993, ApJS, 88, 529
Thompson D. J. et al., 1996, ApJ, 465, 385
Weekes T. C., 1992, Space Sci. Rev., 59, 315